Quantitative MRI and Spectroscopy of Bone Marrow

Dimitrios C. Karampinos, PhD,[1]* Stefan Ruschke, MSc,[1]
Michael Dieckmeyer, MSc,[1] Maximilian Diefenbach, MSc,[1] Daniela Franz, MD,[1]
Alexandra S. Gersing, MD,[1] Roland Krug, MD,[2] and Thomas Baum, MD[3]

Bone marrow is one of the largest organs in the human body, enclosing adipocytes, hematopoietic stem cells, which are responsible for blood cell production, and mesenchymal stem cells, which are responsible for the production of adipocytes and bone cells. Magnetic resonance imaging (MRI) is the ideal imaging modality to monitor bone marrow changes in healthy and pathological states, thanks to its inherent rich soft-tissue contrast. Quantitative bone marrow MRI and magnetic resonance spectroscopy (MRS) techniques have been also developed in order to quantify changes in bone marrow water–fat composition, cellularity and perfusion in different pathologies, and to assist in understanding the role of bone marrow in the pathophysiology of systemic diseases (e.g. osteoporosis). The present review summarizes a large selection of studies published until March 2017 in proton-based quantitative MRI and MRS of bone marrow. Some basic knowledge about bone marrow anatomy and physiology is first reviewed. The most important technical aspects of quantitative MR methods measuring bone marrow water–fat composition, fatty acid composition, perfusion, and diffusion are then described. Finally, previous MR studies are reviewed on the application of quantitative MR techniques in both healthy aging and diseased bone marrow affected by osteoporosis, fractures, metabolic diseases, multiple myeloma, and bone metastases.
Level of Evidence: 3
Technical Efficacy: Stage 2

J. MAGN. RESON. IMAGING 2018;47:332–353.

Bone marrow is encountered in the central cavities of axial and long bones and it is one of the largest body organs, accounting for up to 4–5% of the total body weight in humans. It is composed of a mixture of hematopoietic tissue islands and adipocytes, surrounded by vascular sinuses and interspersed within the network of trabecular bone matrix. It is the major hematopoietic organ and a primary lymphoid tissue. Bone marrow is a dynamic organ with continuous changes taking place with increasing age and altered hematopoietic needs. It is also a target of many pathological changes and diseases affecting its major components (e.g. adipocytes and red blood cells) or its surrounding tissues (e.g. trabecular and cortical bone matrix).

Magnetic resonance imaging (MRI) is the ideal modality to monitor bone marrow changes in healthy and pathological states, thanks to its inherent rich soft-tissue contrast.[1,2] In the routine diagnostic setting, conventional anatomical MRI (ie, T_1-weighted, T_2-weighted, and contrast-enhanced imaging) is being used to diagnose abnormal signal changes in joint injuries and musculoskeletal diseases[3] and to diagnose bone marrow lesions and monitor treatment response in patients with a broad range of pathologies including bone marrow malignancies, bone metastases, multiple myeloma, and compression fractures.[4,5] To overcome the limitations of signal variability in conventional anatomical MR images, quantitative bone

View this article online at wileyonlinelibrary.com. DOI: 10.1002/jmri.25769

Received Mar 29, 2017, Accepted for publication May 5, 2017.

*Address reprint requests to: D.C.K., Department of Diagnostic and Interventional Radiology, Klinikum rechts der Isar, Ismaninger Str. 22, 81675 Munich, Germany. E-mail: dimitrios.karampinos@tum.de

From the [1]Department of Diagnostic and Interventional Radiology, Technical University of Munich, Munich, Germany; [2]Department of Radiology and Biomedical Imaging, University of California, San Francisco, San Francisco, California, USA; and [3]Section for Diagnostic and Interventional Neuroradiology, Technical University of Munich, Munich, Germany

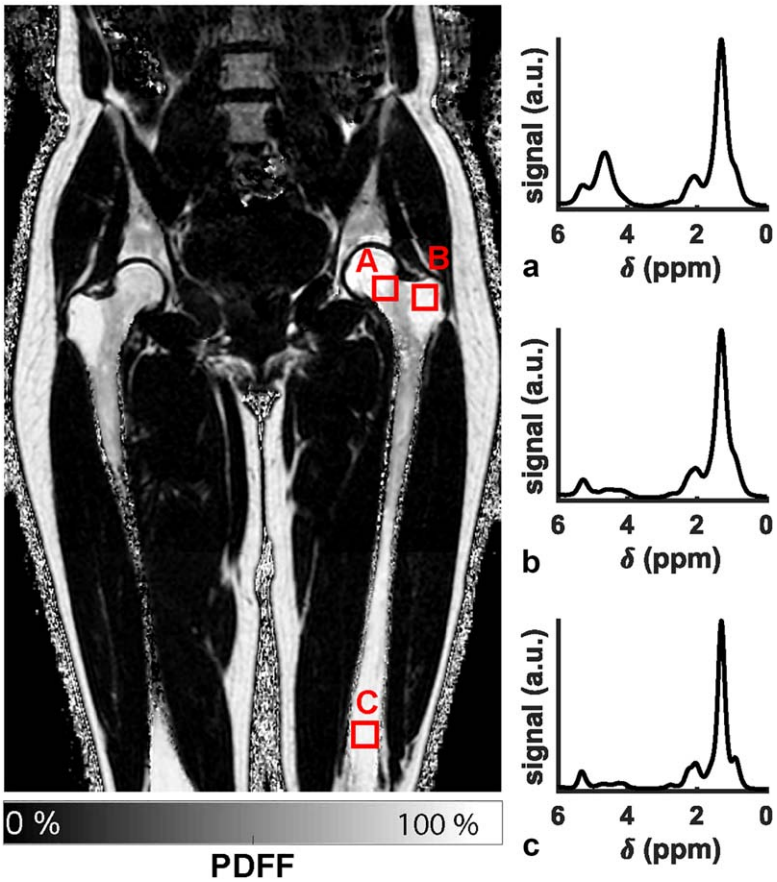

FIGURE 1: Lower spine, pelvis and femurs bone marrow proton density fat fraction (PDFF) map in a 31-year-old female subject and representative bone marrow spectra: (a) in the neck of the proximal femur (red marrow region, broad linewidths, large water peak), (b) in the greater trochanter of the proximal femur (trabecularized yellow marrow region, broad linewidths, small water peak), and (c) in the distal femur (non-trabecularized yellow marrow region, narrow linewidths, small water peak).

marrow MR techniques have been also emerging in order to quantify changes in bone marrow water–fat composition, cellularity and perfusion in different pathologies, and to assist in understanding the role of bone marrow in the pathophysiology of systemic diseases (e.g. osteoporosis, fracture risk in diabetes).

The present review summarizes a large selection of studies published until March 2017 in quantitative MR of bone marrow. In the first part of this article, we review some basic knowledge about bone marrow anatomy and physiology, followed by a description of the most important technical aspects of quantitative MR techniques applied in bone marrow. In the second part of the article, we focus on presenting MR studies applying quantitative MR techniques in both healthy aging and diseased bone marrow.

Literature Search

Electronic searches in PubMed (http://www.ncbi.nlm.nih.gov/pubmed) were performed up to March 2017 to identify relevant studies for the present review. Search terms used included the term "bone marrow" and one of the following terms: "quantitative MRI, MRS, fat fraction, diffusion MRI, perfusion MRI, fat unsaturation, osteoporosis, fractures, multiple myeloma." The search was restricted to studies in humans. The reference lists of relevant articles were also screened.

Bone Marrow Anatomy and Physiology

Bone marrow cavities can be trabecularized or non-trabecularized, depending on their body location. Traditionally, two main types of bone marrow are differentiated: yellow and red bone marrow. The two types of bone marrow have distinct composition and vascularization.

Yellow bone marrow, named after the abundant carotenoid bodies in its fat cells, is primarily composed of fat cells (adipocytes) and its chemical composition is ~80% fat, 15% water, and 5% protein. Yellow bone marrow vasculature is scarce, containing only a few capillaries with continuous basement membrane. Yellow bone marrow is encountered primarily in the appendicular skeleton.

Red bone marrow, named after its richness in hemoglobin and erythrocytes, is composed of both hematopoietic cells and fat cells and its chemical composition can vary but is typically 40–60% lipids, 30–40% water and 10–20% protein. Red bone marrow is responsible for body blood cell production and has a rich vasculature, composed of a vast network of sinusoids. Red bone marrow is found in the

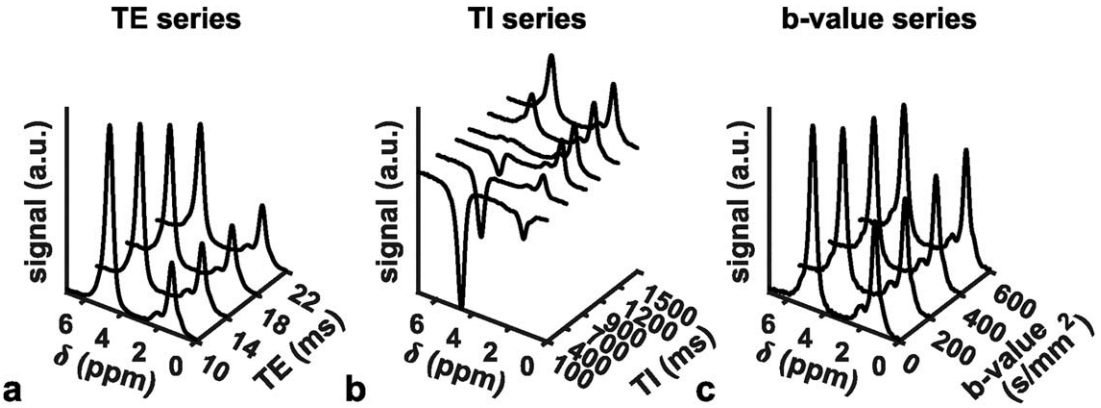

FIGURE 2: Vertebral bone marrow MR spectra (15 × 15 × 15 mm^3 MRS box at the L5 vertebral body) in a 23-year-old female healthy subject with (a) variable T_2-weighting in a STEAM TE series, (b) variable T_1-weighting in an inversion recovery STEAM TI series, (c) variable diffusion-weighting in a diffusion-weighted STEAM b-series. The water peak shows a faster T_2 decay, a slower T_1 recovery and a faster diffusion attenuation compared to the main fat peak.

cavities of the skull, sternum, scapulae, vertebrae, ribs, pelvic bones, and the ends of the long bones near the joints in healthy adults.

Figure 1 shows an example of the bone marrow proton density fat fraction in the lower spine, pelvis, and femurs of a young female subject, and a representative spectrum from a red bone marrow region with trabeculae in the neck of the proximal femur (position a in Fig. 1), a yellow bone marrow region with trabeculae in the greater trochanter of the proximal femur (position b in Fig. 1), and a yellow bone marrow region without trabeculae in the distal femur (position c in Fig. 1).

Red bone marrow is converted to yellow bone marrow with aging in a process that continues throughout life following a pattern from the peripheral towards the central skeleton, as described by Neumann already in 1882.[6] Within an individual bone, red to yellow marrow conversion occurs first in the epiphysis, then in diaphysis, and lastly in metaphysis, following a distal to proximal pattern. The adult red/yellow marrow state is reached around the age of 25 years. At that time, red marrow is restricted to the axial skeleton (spine, sternum, ribs, pelvis, skull) and in the proximal metaphyses of the femur and the humerus. The red to yellow marrow conversion in the axial skeleton continues throughout life and the resulting red marrow distribution over the entire skeleton is in general spatially heterogeneous.

The traditional classification of bone marrow into yellow and red marrow compartments has been based on the presence of hematopoietic cells. In addition, despite the general assumption that all marrow adipocytes are equivalent, in 1976 Tavassoli suggested that red marrow adipocytes may differ from yellow marrow adipocytes.[7] Recent works have further suggested that bone marrow adipose tissue (MAT) can be classified into constitutive and regulated MAT based on the properties of bone marrow adipocytes.[8–10] Specifically, according to the recent work of Scheller et al,[9] regulated MAT (rMAT) refers to single adipocytes interspersed with active hematopoiesis, whereas constitutive MAT (cMAT) has low hematopoiesis, contains larger adipocytes, develops earlier and remains preserved upon systemic challenges.

Technical Aspects of Quantitative Bone Marrow MRI and MRS

We first review the most important technical aspects for quantitative bone marrow MRI and MRS.

Water–Fat Environment

Bone marrow is one of the very few tissues in the human body where both water and fat components can be equally present. The water–fat composition of bone marrow has two important implications when applying quantitative MR in bone marrow. First, MRI and MRS can be used to perform quantitative measurements of the fat fraction and characterize bone marrow water–fat composition. Second, quantitative MRI measurements of individual properties of the bone marrow fat or water components require to suppress or account for the presence of the other component. Figure 2 shows the effect of T_2-weighting, T_1-weighting, and diffusion weighting in representative vertebral bone marrow spectra. Water and fat peaks show different T_2 decay, T_1 recovery, and diffusion attenuation, depending on the underlying different T_2 relaxation times, T_1 relaxation times, and diffusion constants: bone marrow water has typically shorter T_2, longer T_1, and faster diffusion constant than bone marrow fat.[11]

Fat/Water Fraction Quantification

Fat fraction measurements were one of the first examples of quantitative MR techniques applied in vertebral bone marrow in the work by Schick et al in the early 1990s.[12] Since the early applications of MRI and MRS to measure bone marrow signal-weighted fat fraction (SFF), significant

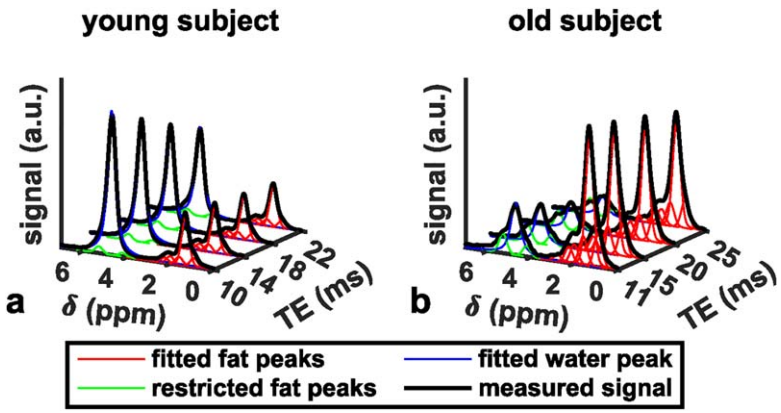

FIGURE 3: Vertebral bone marrow spectra (measured spectra in black) with fitted fat peaks (in red), fitted water peak (in blue) and fat peaks whose peak areas were restricted to the main fat peak area (in green) in (a) a young (23-year-old female) and (b) an old (64-year-old male) subject.

progress has been made in measuring the bone marrow proton density fat fraction (PDFF) in different bone marrow regions, thanks to similar developments occurring in abdominal MR-based fat quantification.[13–16] The goal of most recent technical developments in MR-based fat quantification has been to remove the effect of confounding factors and derive the PDFF, which represents a truly standardized imaging biomarker.[17,18] Two main families of techniques have been emerging for PDFF quantification: single-voxel proton magnetic resonance spectroscopy (MRS) and chemical shift encoding-based water–fat imaging.

SINGLE-VOXEL PROTON MRS. Singe-voxel proton MRS measurements have been extensively applied in measuring the bone marrow fat fraction averaged over a localized region. On the acquisition side, either point-resolved spectroscopy (PRESS) or stimulated echo acquisition mode (STEAM) MRS pulse sequence designs have been mostly employed. When comparing the two sequence designs, STEAM shows two distinct advantages compared to PRESS for the needs of fat quantification. First, STEAM has been shown to have reduced sensitivity to J-coupling effects of the fat peaks compared to PRESS.[19] The reduced sensitivity of STEAM to J-coupling effects of the fat peaks can reduce quantification errors when performing an echo time (TE) series to correct for T_2 decay effects in PDFF quantification.[19] Second, the bone marrow water peak has short T_2. STEAM allows shorter minimum echo times compared to PRESS and despite its 50% signal loss compared to PRESS can reduce the T_2-weighted signal loss for the short T_2 water peak.

Another acquisition consideration, especially when applying single-voxel MRS methods in regions with spatial heterogeneous bone marrow fat fraction distribution (e.g. proximal femur), is that the finite RF pulse bandwidths of the MRS sequence can induce chemical shift displacement effects in MRS voxel localization. For example, by selecting the resonance frequency on the water peak at 3T (chemical shift difference between water and main fat peak = 420 Hz) and with an RF pulse bandwidth of 2777 Hz in a typical STEAM MRS sequence, the chemical shift displacement error for the fat localization equals 15% of the voxel size in each dimension.[20] Such effects can be reduced by selecting the center resonance frequency in the middle between the water peak and the main fat peak (Fig. 2a) or by performing two acquisitions with different center frequencies (one centered at the water and one at the main fat peak).[21] Techniques with improved spatial localization, like semilocalized by adiabatic selective refocusing (semi-LASER), can reduce chemical shift displacement effects but have not been yet applied in bone marrow applications.

In the postprocessing of the acquired bone marrow MR spectra, the complexity of the fat spectrum, T_2 decay effects, potential J-coupling effects, and the presence of broad baseline peaks need to be considered. First, all fat peaks need to be considered in the determination of the PDFF. Bone marrow spectra in trabecularized regions are characterized by broad peaks, complicating robust peak fitting. In order to robustly extract the overlapping water and fat peaks in bone marrow MRS, the absorption spectrum can be characterized on the basis of the magnitude of measurable fat peaks, and an a priori knowledge of the chemical structure of triglycerides should be employed in the MRS peak extraction, as proposed previously in the liver.[22] Such constrained peak fitting methodologies have been recently performed in both the proximal femur and the vertebral bone marrow.[20,21] Figure 3 shows examples of the constrained peak fitting results in the vertebral bone marrow of a young and an old subject. Second, the quantification of the fat fraction based on the acquired spectra has been traditionally performed by acquiring a single TE spectrum.[23–27] However, it has been recently shown that the acquisition of multiple TEs is necessary in order to correct for T_2 decay effects.[20] Finally, short T_2 components can confound the measurement of PDFF from single-voxel MRS as they can induce broad water peaks.[21]

CHEMICAL SHIFT ENCODING-BASED WATER–FAT IMAGING. Chemical shift encoding-based water–fat imaging overcomes the spatial resolution requirements of single-voxel MRS and enables the spatially resolved assessment of bone marrow fat fraction, especially in regions with heterogeneous red marrow distribution (eg, proximal femur, spine). Figure 1 shows an example of the nonuniform spatial distribution of the bone marrow fat fraction in the lower spine, pelvis, and femurs of a young female subject.

On the acquisition side, multiecho gradient echo pulse sequences have been employed using either monopolar or bipolar gradient readouts. To maintain a good noise performance in the water–fat separation, the echo time step of the multiecho gradient echo acquisition needs to result in a water–fat phase difference different from 0 and 2π.[28,29] At 1.5T, the above condition is fulfilled by using sequence designs with monopolar gradient readouts acquiring all echoes in a single TR. At 3T, satisfying the above condition requires using sequence designs either with bipolar gradient readouts acquiring all echoes in a single TR or with monopolar gradient readouts acquiring all echoes in multiple TRs (time-interleaved).

On the postprocessing side, fat quantification techniques rely on parameter estimation based on the complex signal[30] or its magnitude only.[31] Complex-based techniques have been shown to possess superior noise performance compared to their magnitude-based counterparts[32] and lower sensitivity to fat signal modeling errors.[33,34] However, complex-based techniques are also prone to phase errors, induced by concomitant gradients, eddy currents, gradient delays, and other hardware sources.[35,36] Such phase errors can introduce significant PDFF bias spatial patterns that depend on the spatial pattern of the underlying phase errors.[36] For a given phase error, the relative phase error-induced PDFF bias may be in general smaller in bone marrow regions with moderate fat fractions (e.g. close to 50%) compared to regions with high or low fat fractions.[37]

In addition to the effect of phase errors, multiple confounding factors have to be addressed when measuring bone marrow PDFF with water–fat imaging, including the presence of multiple peaks in the fat spectrum,[30,31] T_1-bias,[38,39] and T_2*-decay effects.[29,31] First, the presence of multi-peaks in the fat spectrum should be addressed by incorporating a precalibrated multi-peak fat spectrum in the signal model. Many previous works have used the bone marrow fat spectrum of Ren et al,[40] acquired in yellow bone marrow in the long axis of the tibia at 7T. Mean bone marrow fat spectra have been also derived from constrained peak fitting of single-voxel MRS measurements in bone marrow of the spine[20] and the proximal femur.[21] Susceptibility-induced fat resonance shift effects[41] have not been reported in bone marrow applications. Second, T_1 bias effects can be corrected using estimated T_1 values and flip angle mapping techniques.[42] However, T_1 bias has been most frequently minimized by the selection of a small flip angle.[38,39] Third, the presence of trabecular bone most importantly shortens the T_2* of both the water and fat components, inducing a rapid decay of the measured gradient echo signal with echo time.[21,43,44] T_2* can in general be different between the water and fat components. A dual T_2* correction can improve accuracy in fat fraction estimation, but it reduces the precision in fat quantification.[32] Therefore, approaches with a single T_2* correction[21,45] or with a T_2' correction (where T_2' denotes the reversible spin dephasing relaxation constant) with a priori known water T_2[43] have been used. A dual T_2* correction might be not severely affected by noise effects, when the fat quantification is performed not on a voxel-by-voxel basis but on a region of interest (ROI) level.[46,47] After correcting all confounding effects, a good agreement has been reported in vivo between MRS-based and imaging-based PDFF in both the proximal femur[21] and spine.[43]

Imaging-based and MRS-based bone marrow water and fat fraction measurements have been also validated against chemical analysis[48] and histology.[49–51] Specifically, an ex vivo study using trabecular bone specimens filled with water–fat emulsions of different fat fractions has shown an excellent agreement between imaging-based PDFF and the known PDFF of the emulsions.[48] Arentsen et al[49] and MacEwan et al[51] performed studies comparing water–fat imaging with histological examinations. Water–fat imaging in both studies resulted in vertebral bone marrow fat fraction and water fraction values, which showed good correlation with histological results. MRS-based vertebral bone marrow fat fraction has been also recently shown to be in good agreement with the bone marrow fat fraction from dual-energy computed tomography (CT).[52] Finally, good reproducibility values have been reported for both imaging-based and MRS-based bone marrow fat fraction in the spine[26,53] and the proximal femur.[54,55]

Properties of Fat Component

In addition to measuring the fat fraction, MRS techniques have been employed to measure bone marrow fatty acid composition, with primary applications in osteoporosis and fracture risk assessment. In a typical MR spectrum, the unsaturation and polyunsaturation levels can be extracted from the olefinic (at 5.4 ppm) and diallylic (at 2.8 ppm) fat peak resonances, respectively.[22]

Many previous applications of MRS techniques to measure bone marrow fat unsaturation have focused on vertebral bone marrow using short TE PRESS sequences.[27] The reliable extraction of the olefinic fat peak in vertebral bone marrow spectra is particularly challenging because of the overlapping strong water peak and the general broad linewidths in vertebral bone marrow spectra, especially in

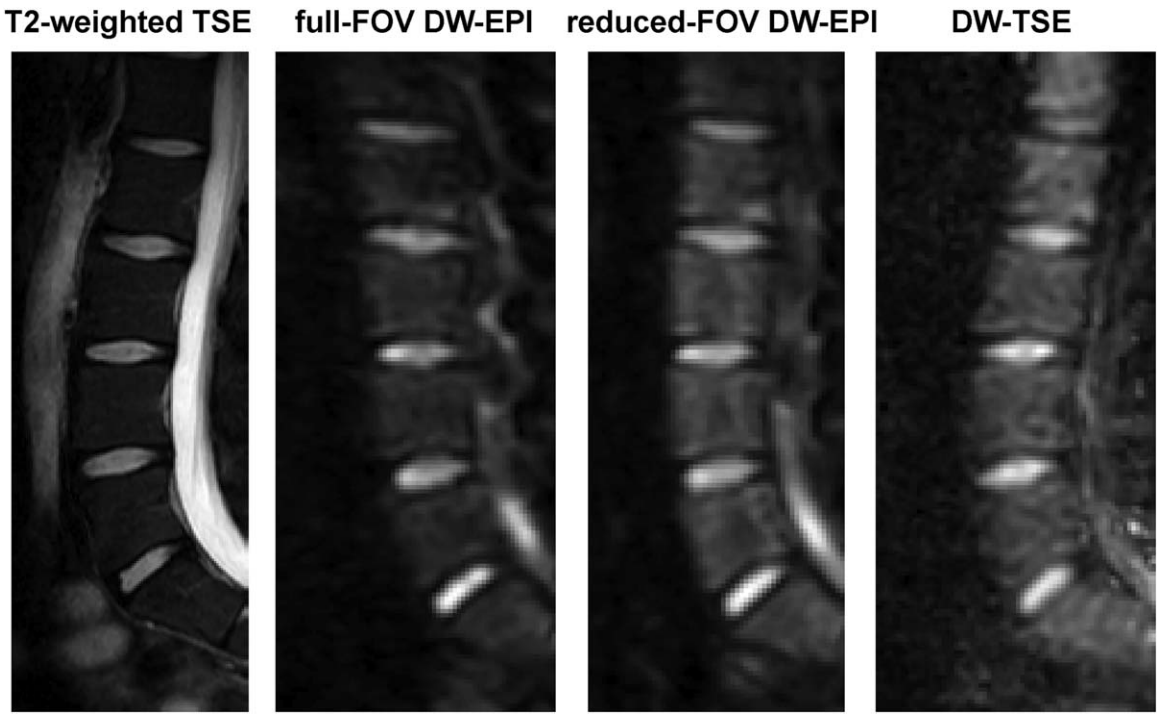

FIGURE 4: Diffusion-weighted imaging of the spine in a 28-year-old male subject: T_2-weighted TSE for anatomical reference, full-FOV DW single-shot EPI (b = 800 s/mm^2), reduced-FOV DW single-shot EPI (b = 800 s/mm^2), single-shot DW TSE (b = 800 s/mm^2). Full-FOV single-shot EPI shows significant geometric distortions, which are reduced in reduced-FOV single-shot EPI and minimized in DW-TSE. DW-TSE shows increased blurring.

younger subjects (Fig. 3). Therefore, vertebral bone marrow fat unsaturation results based on short TE PRESS have shown relatively poor reproducibility.[26] In addition, previous vertebral bone marrow fat unsaturation results based on short TE PRESS have not accounted for J-coupling effects.

The olefinic and diallylic protons, like most lipid protons, are affected by J-coupling interactions.[19] Minimization of such J-coupling interactions is critical in order to reliably quantify unsaturation and polyunsaturation levels based on the olefinic an diallylic fat peaks. Previous work in adipose tissue[56] and liver[57] has shown that PRESS with TE = 135 msec and PRESS with TE = 200 msec are suitable at 1.5T for minimizing J-coupling effects for the diallylic and olefinic fat peaks, respectively. Recent work in vegetable oils and bone marrow has shown that PRESS with TE = 200 msec[58] and STEAM with TE = 100 msec and TM = 20 msec are also suitable at 3T for minimizing J-coupling effects for the olefinic fat peak.[59]

Properties of Water Component

Relaxation, diffusion, perfusion, and magnetization transfer properties of the bone marrow water component have been previously reported.

T_1 AND T_2 RELAXATION. Early T_1 and T_2 relaxation time measurements of the vertebral water component were reported by Schick et al at 1.5T using MRS measurements.[11] Recent work using T_2-corrected MRS for the estimation of vertebral PDFF has also resulted in water T_2 relaxation times at 3T.[20] An interesting inverse correlation between water T_2 relaxation time and PDFF has been reported at both 1.5T[60] and 3T.[20] A possible explanation of this result may be related to differences in water-cellular composition.

DIFFUSION. Diffusion-weighted imaging (DWI) can provide information about tissue microstructure with broad applications in bone marrow diseases, including diagnosing and monitoring bone marrow tumors and differentiating benign from malignant fractures.[61,62] However, application of DWI in bone marrow faces some important technical challenges.

On the acquisition side, single-shot spin-echo echo planar imaging (EPI) sequences have been primarily used in most body applications, thanks to their robustness to motion effects. However, bone marrow regions are mostly included within cortical bone structures and given the magnetic susceptibility difference between bone and tissue water/fat, significant off-resonance effects occur when applying single-shot EPI for bone marrow DWI. Such off-resonance effects induce geometric distortions, especially as the spatial resolution increases (Fig. 4). Parallel imaging techniques can reduce the effect of geometric distortions, but their application depends on the coil sensitivity profiles of the employed coil array and is not always feasible (e.g. in the spine). One alternative technique previously applied in vertebral bone marrow imaging is single-shot reduced-field of view (FOV) EPI. Reduced-FOV imaging can be achieved by using outer volume suppression pulses[63] or 2D RF

excitation pulses.[64,65] Single-shot reduced-FOV EPI can reduce geometric distortion effects (Fig. 4), but reduces signal-to-noise ratio (SNR) and therefore require longer scan times. DW single-shot turbo-spin-echo (TSE) imaging can also minimize geometric distortions. To remove the effect of motion-induced phase errors in violating the Carr–Purcell–Meiboom–Gill (CPMG) condition, DW single-shot TSE requires the application of dephasing gradients as proposed by Alsop, which results in a 50% signal loss.[66] In addition, DW single-shot TSE suffers from increased T_2 blurring (Fig. 4). DW steady-state free-precession techniques have also shown good results in bone marrow applications.[62] Their implementation is primarily challenged by the difficulties on relating the measured signal to the diffusion coefficient.[67] A visual comparison of 3T DW images of the lumbar spine with single-shot reduced-FOV EPI, single-shot reduced-FOV EPI, and single-shot TSE is shown in Fig. 4.

On the diffusion signal modeling side, the effect of the presence of fat should be considered when applying DWI in bone marrow. In order to extract the apparent diffusion coefficient (ADC) of the water component, all fat signals need to be adequately suppressed. Traditional spectral suppression techniques can suppress the main fat peaks, but cannot suppress the olefinic and glycerol fat peaks (which have a resonance frequency in the proximity to the water peak). The incomplete olefinic/glycerol fat peaks suppression effect has been previously shown in DWI of skeletal muscle[68,69] and fatty infiltrated liver.[70] Dieckmeyer et al recently characterized the effect of the incomplete olefinic/glycerol fat peaks suppression in vertebral bone marrow DWI and proposed a methodology to reduce the associated bias.[71] Techniques using an echo time-shifted DW acquisition approach coupled with a water-olefinic fat separation approach have been also recently proposed for skeletal muscle applications,[68,72] but not yet applied in bone marrow.

PERFUSION. Perfusion MRI can provide information about bone marrow hemodynamic parameters, including blood volume, blood flow, and transit time constants. Perfusion has been extensively applied to study alternations in bone marrow perfusion using dynamic contrast-enhanced (DCE) MRI techniques.[61] DCE-MRI relies on the acquisition of contrast-media-induced signal increase in a T_1-weighted acquisition.

Perfusion parameters can be extracted by semiquantitative or quantitative analysis of the T_1-weighted signal. Semiquantitative analysis involves the extraction of descriptive parameters like the maximum enhancement or the slope of the signal–time curve. Quantitative analysis requires the additional measurement of an arterial input function and a tracer kinetic analysis to derive perfusion and permeability parameters. Previous works have primarily employed semiquantitative analysis on bone marrow DCE data[23] and there are only a few studies using quantitative analysis tools and especially addressing the effect of the presence of the fat signal on the extracted perfusion metrics.[73]

MAGNETIZATION TRANSFER. Pulsed magnetization transfer (MT) modules have been combined with PRESS spectroscopy pulse sequences to measure the magnetization transfer of the water component in hematopoietic red marrow.[74] Spectra were acquired with and without MT prepulses. Water peak signals from marrow with increased content of extracellular water due to inflammation or edema revealed less magnetization transfer effects than marrow with increased intracellular water content due to cellularity differences.[74]

Properties Related to Trabecular Bone Matrix

Quantitative bone marrow MRI has been also applied to indirectly measure properties of the trabecular bone matrix. High-resolution MRI can achieve sufficient spatial resolution to depict trabecular bone structure in peripheral skeletal locations,[75] but suffers from low SNR in the spine and the red bone marrow of the proximal femur.[76] An alternative approach for measuring trabecular bone matrix properties is by quantifying the line broadening of the bone marrow protons, induced by the magnetic susceptibility difference between trabecular bone matrix and bone marrow. The reversible spin dephasing relaxation constant R_2' in trabecularized bone marrow has been shown to depend on the trabecular volume fraction[77] and trabecular orientation.[78] The measurement of R_2' has been previously achieved by acquiring a series of gradient echoes around a spin echo.[79] The reliable extraction of R_2' in trabecularized bone marrow requires further addressing the presence of multiple fat peaks in yellow marrow regions[80] and the presence of multiple fat peaks and the water peak in red marrow regions.[81]

Applications of Quantitative Bone Marrow MRI and MRS

We next review the most important applications of quantitative MRI and MRS in characterizing bone marrow changes in healthy aging and different pathological states.

Healthy Aging

Aging-associated changes in bone marrow have been characterized based primarily on fat fraction and perfusion measurements. Multiple studies have investigated the anatomic, age, and gender variance of vertebral bone marrow fat fraction using single-voxel proton MRS and chemical shift encoding-based water–fat imaging.[82–88] Baum et al performed water–fat imaging of the entire spine in 28 young, healthy subjects (17 males, 11 females, age: 26 $\pm$ 4 years).[83] They observed an increase of vertebral bone marrow PDFF from the cervical to the lumbar spine. Furthermore, an age-related increase of vertebral bone marrow signal-weighted fat fraction was demonstrated in different sample sizes, eg, 20 males (age range: 30–65 years) and 24 females (age range:

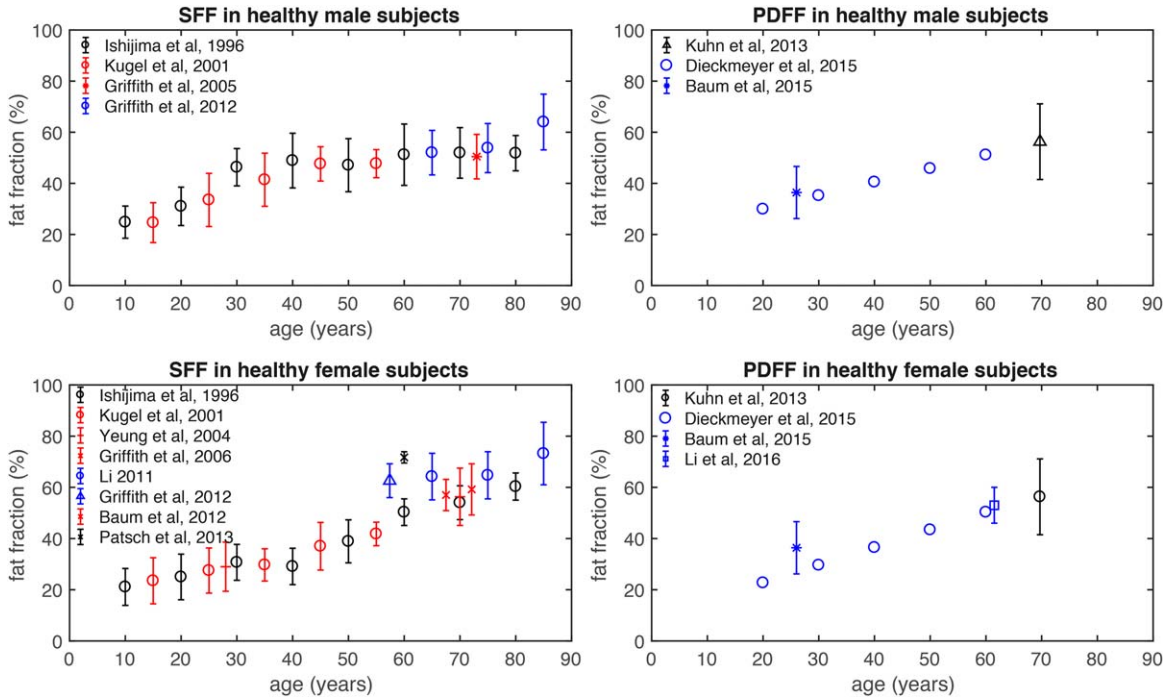

FIGURE 5: Age dependence of vertebral signal-weighted fat fraction (SFF) in left column and proton density fat fraction (PDFF) in right column for healthy male subjects (upper row) and healthy female subjects (lower row), as reported in previous studies. Errors bars indicate fat fraction standard deviation.

30–69 years),[87] 154 healthy subjects (age range: 11–95 years),[85] and 259 healthy subjects (age range: 62–90 years).[84] These studies also observed a gender variance of the vertebral bone marrow fat, with greater values in male compared to female subjects. However, Griffith et al reported a reversal of these gender differences over the age of 60 years.[84] Vertebral bone marrow fat content in females over the age of 60 years was 10% greater than in males of the same age. The authors hypothesized that this finding results from an android pattern of fat deposition in postmenopausal women. A major challenge in grouping the results from all the above previous works is the derivation of a signal-weighted fat fraction, instead of the PDFF, and the dependence of the extracted signal-weighted fat fraction on the employed acquisition and data analysis (Fig. 5).

In consistency, female subjects demonstrated a greater marrow perfusion rate than men younger than 50 years and a more marked decrease than men older than 50 years.[89] Furthermore, MR perfusion amplitude decreased with age and showed an anatomical variance with a decrease from L1 to L5.[90] Lastly, little is known about the age-related changes of bone marrow diffusion. Hillengass et al reported no significant correlation of ADC of the lumbar bone marrow with age, while Yeung et al observed reduced ADC values in older women with normal BMD compared to young, healthy controls.[90,91]

Primary Osteoporosis

CLINICAL BACKGROUND. Osteoporosis is defined as a skeletal disorder characterized by compromised bone strength predisposing an individual to an increased risk for fracture.[92] Osteoporotic fractures, particularly at the spine and hip, are associated with a high mortality rate and generate immense financial costs.[93,94] The assessment of fracture risk has traditionally relied on the measurements of bone mineral density (BMD) by using dual-energy X-ray absorptiometry (DXA). However, BMD values of subjects with versus without osteoporotic fractures overlap.[95,96] Therefore, the Fracture Risk Assessment Tool (FRAX) has been introduced which uses easily obtainable clinical risk factors to estimate a 10-year fracture probability in order to provide a better clinical guidance for treatment decisions.[97] Furthermore, extensive imaging research has been performed to assess the microarchitecture of the mineralized bone component by using high-resolution CT and MRI. Multiple studies demonstrated the ability of bone microstructure parameters as surrogate marker of bone quality to improve fracture risk prediction beyond BMD.[98,99] The bone marrow as a nonmineralized bone component has recently drawn attention with regard to the pathogenesis of osteoporosis.[100,101] The bone marrow affects bone metabolism in several ways. Most important, from the imaging perspective, pluripotent mesenchymal stem cells have the potential to differentiate to osteoblastic and adipocytic cell lines.[102] The composition of the bone marrow therefore shifts towards the presence of adipocytes with both increasing age and osteoporosis. Table 1 summarizes the most important effects previously reported in quantitative bone marrow MRI studies of osteoporosis.

TABLE 1. Summary of Most Important Effects Shown in Quantitative Bone Marrow MRI Studies of Osteoporosis

Effect	Study	Subjects	MRI/MRS technique
Fat fraction			
Fat fraction ↑ in osteoporosis	Yeung et al, 2005	53 women	SFF with single-voxel PRESS (TE = 25 msec, 1.5T)
Fat fraction ↑ in osteoporosis	Griffith et al, 2005	90 men	SFF with single-voxel PRESS (TE = 25 msec, 1.5T)
Fat fraction ↑ in osteoporosis	Griffith et al, 2006	103 women	SFF with single-voxel PRESS (TE = 25 msec, 1.5T)
Fat fraction ↑ in osteoporosis	Li et al, 2011	51 women	SFF with single-voxel PRESS (TE = 37 msec, 3T)
Fat fraction ↑ in osteoporosis	Kühn et al 2013	51 subjects	PDFF with water–fat imaging (3T)
Fat fraction positively associated with prevalent vertebral fracture in men, even after adjustment for BMD	Schwartz et al, 2013	257 subjects	SFF with single-voxel PRESS (TE = 37 msec, 1.5T)
Fat fraction negatively associated with failure load	Karampinos et al 2015	10 specimens	PDFF with single-voxel STEAM (3T)
Fat fraction negatively associated with BMD	Li et al, 2016	83 subjects	PDFF with water–fat imaging (3T)
Fat unsaturation			
Fat unsaturation ↓ in osteoporosis	Yeung et al, 2005	53 women	single-voxel PRESS (TE = 25 msec, 1.5T)
Fat unsaturation negatively associated with prevalence of fragility fractures	Patsch et al 2013	69 women	single-voxel PRESS (TE = 37 msec, 3T)
Diffusion			
ADC ↓ in osteoporosis	Yeung et al, 2004	64 women	Single-shot DW EPI (1.5T)
ADC negatively associated with fat fraction	Griffith et al, 2006	103 women	Single-shot DW EPI (1.5T)
ADC ↓ in osteoporosis	Hatipoglou et al, 2007	51 subjects	Single-shot DW EPI (1.5T)
Perfusion			
Enhancement slope ↓ in osteoporosis	Griffith et al, 2005	82 men	DCE-MRI (1.5T)
Enhancement slope ↓ in osteoporosis	Griffith et al, 2006	103 women	DCE-MRI (1.5T)
Enhancement slope ↓ and maximum enhancement ↓ in osteoporosis	Griffith et al, 2008	120 women	DCE-MRI (1.5T)

FAT FRACTION. Karampinos et al examined 10 vertebrae from human cadavers using single-voxel ^{1}H-MRS to assess vertebral bone marrow PDFF and compared these measurements with CT-based BMD and trabecular bone microstructure parameters, and biomechanically assessed vertebral bone strength.[103] They reported significant correlations between the MRS-based PDFF and multidetector CT (MDCT)-based parameters (up to $r = -0.72$), and between MRS-based fat PDFF and vertebral failure load ($r = -0.77$). That study demonstrated that bone marrow PDFF is negatively associated with BMD, trabecular bone microstructure, and bone strength. Griffith et al performed one of the first large-scale in vivo studies comparing vertebral bone marrow fat content using single-voxel proton MRS in older men and women with varying BMD assessed by DXA.[23,24] They recruited 82 male subjects (mean age of 73 years; age range of 67–101 years).[23] Forty-two subjects had normal BMD, 23 subjects were osteopenic, and 17 subjects were classified as osteoporotic based on DXA measurements. Vertebral bone marrow signal-weighted fat fraction in L3 was significantly increased in subjects with osteoporosis (58.2% ± 7.8%) and osteopenia (55.7% ± 10.2%) compared to that of subjects with normal BMD (50.4% ± 8.7%). Similarly, in 110 postmenopausal women (mean age of 73 years; age range of 67–84 years) single-voxel proton MRS-based vertebral bone marrow signal-weighted fat fraction was significantly elevated in osteoporotic subjects (67.8% ± 8.5%) compared to that in subjects with normal BMD (59.2% ± 10.0%).[24] Li et al performed single-voxel ^{1}H-MRS in six subjects twice at four vertebral body levels (L1–L4) on the same day with repositioning between the two scans.[26] They reported a good reproducibility of proton MRS-based vertebral bone marrow signal-weighted fat fraction measurements with an averaged coefficient of variation of 1.7%.

Another method recently applied for measuring bone marrow PDFF in osteoporosis is quantitative chemical shift encoding-based water–fat imaging. Figure 6 shows the increasing PDFF values in PDFF maps of the lumbar spine in a 74-year-old healthy woman, a 57-year-old osteopenic woman, and a 59-year-old osteoporotic woman. Figure 7 shows the decreasing trabecular structure and the increasing PDFF values in proximal femur high-resolution trabecular bone images and corresponding PDFF maps of three postmenopausal women with increasing osteoporotic status according to DXA.

Different studies reported an association of osteoporosis with water–fat imaging-based PDFF.[44,104,105] Kühn et al studied 51 patients (28 female; mean age 69.7 ± 9.0 years) who underwent DXA from L1 to L4 to measure BMD and chemical shift chemical encoding-based water–fat imaging to determine vertebral bone marrow PDFF.[44] The vertebrae were divided into three groups (healthy, osteopenic, and osteoporotic) based on the DXA-derived *t*-score. The area under the curve to differentiate between normal and osteoporotic vertebrae was statistically significant, with an area under the curve of 0.656. Water–fat imaging offers the clear advantage that vertebral bone marrow fat quantification can be performed over a large range of the spine in an acceptable scan time, e.g. stacks of the cervical, thoracic, and lumbar spine with 3–4 minutes for each stack, respectively.[83,106] Reproducibility of water–fat imaging-based PDFF has been reported to be excellent, e.g. absolute precision error of PDFF averaged over C3–L5 amounted to 1.7%.[82,83]

Schwartz et al have shown that higher marrow fat correlated with lower trabecular BMD in older women but not men and that higher marrow fat was associated with prevalent vertebral fracture in men, even after adjustment for BMD.[107] However, the performance of bone marrow PDFF quantification as an imaging biomarker beyond BMD remains still unclear and has to be further investigated in the future.

Figure 8 summarizes the most important previous studies measuring bone marrow fat fraction differences using MRS or imaging between healthy and osteoporotic subjects. Fat fraction differences between healthy and osteoporotic subjects have been previously based primarily on SFF measurements employing different experimental settings and data analysis techniques, resulting in a large variability on the reported fat fraction values (Fig. 8).

FATTY ACID COMPOSITION. The bone marrow fat unsaturation level has been also employed in osteoporosis assessment. Yeung et al recruited 53 older women (mean age of 70 years) and 12 young female controls (mean age of 28 years) who underwent DXA and single-voxel ^{1}H-MRS of the lumbar spine.[27] Water and lipid peak amplitudes were measured to determine vertebral bone marrow fat content and fat unsaturation level. Marrow fat fraction was significantly increased in osteoporotic (65.5% ± 10.0%) and osteopenic (63.5% ± 9.3%) subjects compared to normal subjects (56.3% ± 11.2%) and young controls (29.0% ± 9.6%). The fat unsaturation level was significantly decreased in osteoporotic (0.091 ± 0.013) and osteopenic (0.097 ± 0.014) subjects compared to normal subjects (0.114 ± 0.016) and young controls (0.127 ± 0.031). Furthermore, an inverse correlation was reported between the fat content and the unsaturation level ($r = -0.53$). Patsch et al performed single-voxel ^{1}H-MRS at the lumbar spine in diabetic and nondiabetic postmenopausal women with and without fragility fractures.[108] Consistent with Yeung et al, the prevalence of fragility fractures was associated with –1.7% lower unsaturation levels and +2.9% higher saturation levels, while BMD measurements could not differentiate between fracture and nonfracture subjects.

DIFFUSION. Beyond proton MRS and chemical shift encoding-based water–fat MRI, MR diffusion imaging has

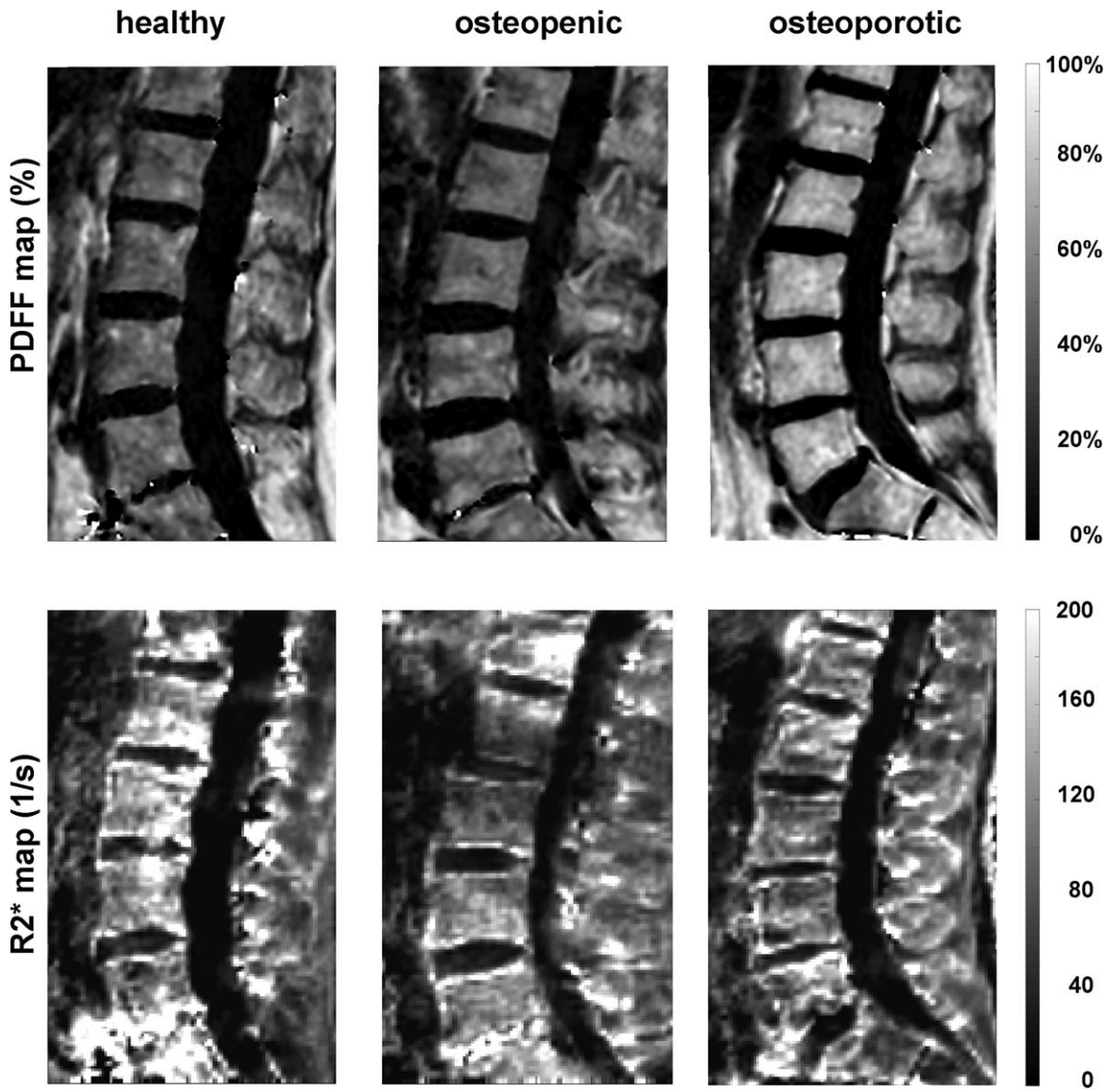

FIGURE 6: PDFF and R_2* maps of the lumbar spine in a 74-year-old healthy woman (left column), a 57-year-old osteopenic woman (middle column), and a 59-year-old osteoporotic woman (right column). Osteoporosis status assessed based on DXA of the lumbar spine. PDFF increases and R_2* decreases with increasing osteoporosis status, consistent with an increase in bone marrow fat fraction and a decrease in trabecular bone density.

been also applied for the detection of osteoporosis-related changes in the bone marrow. Yeung et al performed one of the first studies investigating whether quantitative MR diffusion imaging reveals differences between subjects with postmenopausal osteoporosis and premenopausal controls.[91] They recruited 44 consecutive women (mean age: 70 years) subdivided by DXA-based *t*-score and 20 controls (mean age: 28 years). They were examined with echo-planar diffusion imaging at 1.5T using b values of 0, 20, 40, 60, 80, 100, 200, 300, 400, and 500 s/mm^2. Extravascular diffusion (D) and ADC were significantly decreased in osteoporotic subjects compared to controls, indicating increased diffusion restriction effects induced by the accumulation of fat cells due to osteoporosis. Further studies confirmed this finding with correlation of *t*-score and ADC up to $r = 0.835$.[109–111] However, Griffith et al observed no significant ADC differences in the vertebral bone marrow between 18 female subjects with normal BMD, 30 females with DXA-based osteopenia, and 55 female subjects with DXA-based osteoporosis.[24] In the light of these conflicting results, the relevance of MR diffusion imaging as an imaging biomarker for osteoporosis diagnostics remains unclear.

PERFUSION. The motivation of MR perfusion imaging in the context of osteoporosis is based on the pathophysiological changes in the osteoporotic bone with an increase in marrow fat and a reduction of bone marrow arteries and capillary sinusoids.[112] Griffith et al recruited 82 male subjects (age range: 67–101 years) with normal, osteopenic, and osteoporotic DXA-based BMD status.[23] They observed significantly

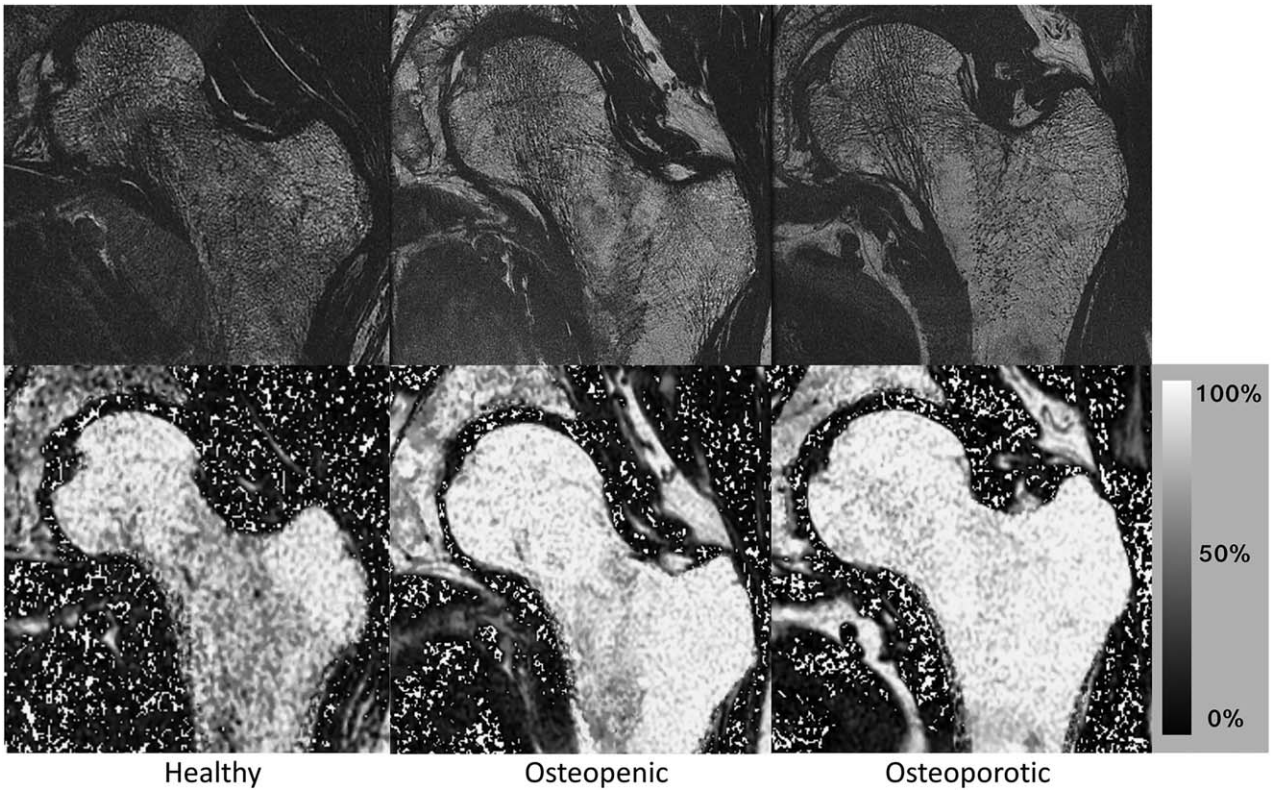

FIGURE 7: Proximal femur high-resolution trabecular bone images (234 × 234 × 500 μm^3) and PDFF maps in the proximal femur of a healthy postmenopausal woman (left column), in an osteopenic postmenopausal woman (middle column), and in an osteoporotic postmenopausal woman (right column). Osteoporosis status was assessed based on DXA of the hip. A decrease in trabecular bone structure can be appreciated with increasing osteoporotic status (note in particular the larger areas of bone marrow in the femoral neck). The PDFF maps show a trend to higher bone marrow fat fractions with osteoporotic status. Also of note, the greater trochanter and the femoral head show high PDFF values in all three subjects, whereas the femoral neck PDFF varies from lower values (healthy subject) to very high values in the patient with osteoporosis.

decreased enhancement slope in the osteoporotic group (1.10%/sec ± 0.51%/sec) compared to the osteopenic group (1.45%/sec ± 0.51%/sec) and normal BMD group (1.70%/sec ± 0.52%/sec). Similar findings were reported in further studies investigating the vertebral bone marrow perfusion properties in postmenopausal women.[24,113] MR perfusion imaging at the proximal femur revealed consistent results. Griffith et al performed MR perfusion imaging in 120 female subjects (mean age: 74 years) and observed in the femoral head, neck, shaft, and the acetabulum reduced maximum enhancement and enhancement slope in subjects with osteoporosis compared to those with osteopenia or normal BMD.[114] Furthermore, reduced bone perfusion in proximal femur preferentially affected the femoral neck in osteoporotic subjects.[115] This is of particular interest, as the femoral neck is one of the clinically most important fracture sites in osteoporosis. However, MR perfusion imaging as well as all the above-mentioned MR techniques lacks the evidence to be more predictive for bone loss than traditional risk factors, thus limiting so far their application in clinical practice.

Metabolic Diseases

Quantitative MRI and MRS of the bone marrow has emerged as a useful tool in evaluation of metabolic diseases, as various studies suggest an association of bone marrow adiposity with metabolism.

Studies on changes of bone marrow fat in metabolic diseases have predominantly used single-voxel MRS for bone marrow fat quantification. In obesity, single-voxel MRS showed that bone marrow fat is positively associated with visceral fat and inversely associated with bone mineral density and insulin-like growth factor 1 in obese women, stressing the detrimental effect of visceral fat on bone health.[116] In addition, bone marrow fat has been shown to be positively associated with ectopic and serum lipids in obese subjects.[117] However, in a dietary intervention study in obese women, MRS-determined bone marrow fat fraction was not statistically significantly changed after the intervention.[118] In another recent study, bone marrow fat changes were observed after gastric bypass surgery only in women with diabetes compared to nondiabetic women.[119]

Moreover, in women with type 2 diabetes mellitus, MRS-based vertebral bone marrow fat correlated significantly with visceral adipose tissue and HbA1c levels, indicating that vertebral bone marrow fat content might be used as a biomarker for glycemic control. Men with diabetes had a higher bone marrow fat fraction compared to nondiabetic men. The correlation between bone marrow fat fraction and BMD

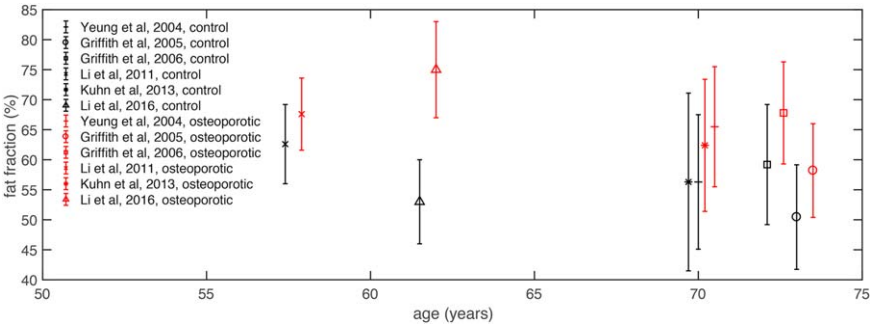

FIGURE 8: Comparison of the vertebral fat fraction (SFF and PDFF plotted together) between healthy subjects (control, in black) and osteoporotic subjects (in red) as a function of age in previous studies. Errors bars indicate fat fraction standard deviation.

differed by diabetes status.[120] With regard to fatty acid composition, a lower fat unsaturation in bone marrow fat was found in diabetic women compared to nondiabetic women.[121] In women with anorexia nervosa, Bredella et al were able to demonstrate a paradoxical increase in bone marrow fat measured via single-voxel MRS, with higher fat fraction in anorectic women compared to healthy controls.[122]

With MRS being a rather time-consuming method, limited in spatial resolution, chemical shift-encoding based water–fat MRI was used to determine bone marrow fat fraction in a study by Slade et al, showing that bone marrow adiposity was not increased in type 1 diabetes while there was a striking positive correlation between marrow adiposity and serum lipid levels.[123] Grey et al used both MRS and water–fat imaging to measure changes of bone marrow fat in patients with type 2 diabetes mellitus with and without short-term treatment with pioglitazone and found an increase in bone marrow fat with both techniques in the pioglitazone group.[124]

Differentiating benign versus malignant fractures

CLINICAL BACKGROUND. The differentiation between benign osteoporotic and malignant fractures is crucial for individual therapy decision and diagnostic follow-up. A previous study has shown that in 5% of patients undergoing vertebroplasty after an assumed osteoporotic fracture, malignant tissue was found by histology.[125] This underlines the necessity to assess fractures with imaging modalities with the highest sensitivity and specificity in order to ensure proper diagnosis before treatment. Since fractures associated both with osteoporosis and bone metastases often occur in elder individuals, mostly without adequate trauma, the clinical differentiation between the two fracture types is challenging. Morphological MRI can provide information on the configuration of the bone, adjacent structures, and soft tissue as well as on bone marrow signal abnormalities representing, e.g. bone bruise or cellular infiltration and thus is superior to radiography and CT. Certain aspects of the mentioned morphological criteria have shown moderate to high sensitivity and specificity in the differentiation between, e.g. malignant and osteoporotic vertebral fractures in previous studies.[126,127] Nevertheless, in cases in which features of both categories, malignant and osteoporotic fractures, are found, novel MRI techniques may be more accurate for differentiating between the two fracture types. Table 2 summarizes the most important effects shown in quantitative bone marrow MRI studies for differentiating benign versus malignant fractures.

FAT FRACTION. In-phase and opposed-phase imaging has been traditionally used to semiquantitatively assess water–fat composition changes in fractured skeletal sites. Normal bone marrow and marrow in vertebrae with osteoporotic fractures show a signal intensity loss between the in-phase and following opposed-phase images due to a balanced composition of bone marrow consisting of almost equal amounts of fat and water.[128] Malignant processes are associated with the replacement of normal bone marrow fat by cancer cells with a consequent lack of signal intensity loss in the opposed-phase images compared to the in-phase images.[129,130] Previous studies have calculated a cutoff of 0.75–0.8 for the ratio of opposed-phase signal to the in-phase signal in order to differentiate between malignant and benign processes in fractured vertebra.[129,130] It has also recently been shown that the fat fraction based on chemical-shift encoding-based water–fat imaging could be used to allow a distinction between benign and malignant causes of focal bone marrow abnormalities when difficulty in the qualitative interpretation of conventional MR image arises.[131]

DIFFUSION. Diffusivity is reduced in tissue with a high cellularity, e.g. in bone marrow invaded by tumor cells, due to a reduction of the extracellular fluid component.[132] Consequently, malignant fractures present with a hyperintense signal on DW images, whereas benign fractures show less reduction in diffusivity and therefore present with an iso- or hypointense DWI signal. Bone marrow signal may vary on DWI due to, e.g. changes induced by radiation therapy; therefore, the signal of fractured bone structures needs to be assessed in relation to bone marrow of adjacent unaffected regions in order to avoid misinterpretation.[133] Moreover, bone marrow edema, which is initially present in every

TABLE 2. Summary of the Most Important Effects Shown in Quantitative Bone Marrow MRI Studies for Differentiating Benign Versus Malignant Fractures

Effect	Study	Subjects	MRI/MRS technique
Fat fraction			
Fat fraction ↓ in malignant compared to benign lesions	Yoo et al, 2016	120 patients	PDFF with water–fat imaging (3T)
Diffusion			
ADC ↓ in malignant compared to benign lesions	Yeung et al, 2004	46 patients	Single-shot DW TSE (1.5T)
ADC ↓ in malignant compared to benign lesions	Dietrich et al, 2015	Meta-analysis	Meta-analysis of 16 previous studies (1.5T–3T)
Perfusion			
Peak enhancement ↑ in malignant compared to benign fractures	Tokuda et al, 2005	34 patients	DCE-MRI (1.5T)
Extracellular volume ↓ in malignant compared to benign fractures	Geith et al, 2013	44 patients	DCE-MRI (1.5T)

fractured bone structure to a certain extent, induces long T_2 relaxation times, and since isotropic DWI is a T_2-based technique, the so-called T_2 shine-through effect, may be misleading in benign fractures. ADC mapping instead removes T_2 shine-through effects. Using a DW single-shot TSE sequence, ADC calculated with b = 100, 250, and 400 s/mm^2 provided the best diagnostic performance with a sensitivity of 85% and a specificity of 84.6%, using an ADC cutoff of 1.7×10^{-3} mm^2/s or less in order to differentiate a malignant vertebral fracture from a osteoporotic vertebral fracture.[134] In a recent meta-analysis of previously published studies, osteoporotic vertebral fractures demonstrate significantly greater ADC values (typically between 1.2 and 2.0×10^{-3} mm^2/s) than malignant vertebral fractures or lesions (typically between 0.7 and 1.3×10^{-3} mm^2/s).[62] DWI sequences without and with conventional fat saturation are in general highly influenced by bone marrow fat content,[61] causing low signal in fat-containing bone marrow which may lead to misinterpretation in the differentiation of malignant and benign processes within the bone marrow.

PERFUSION. Bone marrow with malignant processes and fractures reportedly showed increased slope and maximum enhancement in comparison to benign fractures.[135] Of note, interindividual variations of water and fat content within the different bone marrow regions reduce sensitivity and specificity, which is a limitation of this technique. In order to overcome this limitation, a quantitative assessment of bone perfusion and permeability of the bone marrow has been investigated.[136] A current study showed significantly lower interstitial volume in malignant fractures and lower extracellular volume calculated using DCE images, compared to osteoporotic fractures.[137] Moreover, extraction flow was shown to be significantly lower in malignant fractures compared to osteoporotic fractures with a cutoff of 6.52 mL/100 mL/min or less.[137]

Hematological Diseases and Multiple Myeloma

MRI and MRS of bone marrow have been applied in the early years in the assessment of bone marrow cellularity (using fat fraction, diffusion, or magnetization transfer measurements) in patients with leukemia undergoing therapy or receiving bone marrow transplantation.[138,139] Recently, quantitative MRI of bone marrow has been increasingly applied in patients with multiple myeloma. Table 3 summarizes the most important effects shown in quantitative bone marrow MRI studies in multiple myeloma.

CLINICAL BACKGROUND. Multiple myeloma (MM) is a hematological malignancy with the disease evolving from an asymptomatic stage, the monoclonal gammopathy of undetermined significance (MGUS) to smoldering multiple myeloma (SMM), and finally to MM. MM is characterized by a proliferation of monoclonal plasma cells in bone marrow and may ultimately result in symptomatic MM causing symptoms such as anemia and bone disease.[140,141] Aside from the detection of monoclonal proteins in serum or urine, the detection of bone lesions is one of the main diagnostic criteria listed by the International Myeloma Working Group.[142] Currently, MM is defined by the presence of a lesion (>5,mm) detected on morphological MR imaging,[142] yet previous studies have suggested including information on bone marrow composition and vascularization in addition to tumor size measurement for therapy monitoring in patients with MM.[143,144] For the detection of bone marrow

TABLE 3. Summary of the Most Important Effects Shown in Quantitative Bone Marrow MRI Studies in Multiple Myeloma

Effect	Study	Subjects	MRI/MRS technique
Diffusion			
ADC ↑ in treatment responders	Horger et al, 2011	12 patients	Single-shot DW EPI (1.5T)
ADC ↑ in tumors compared to yellow and red marrow	Padhani et al, 2013	39 patients	Single-shot DW EPI (1.5T)
Negative correlation between change in ADC and change in laboratory markers of treatment response	Giles et al, 2014	34 patients	Single-shot DW EPI (1.5T)
Perfusion			
Time intensity curve parameters can differentiate between different MM groups	Dutoit et al, 2013	219 patients	DCE-MRI (1.5T)

infiltration, before bone destruction has occurred, MRI remains the most sensitive imaging modality.[145] Conventional T_1-weighted spin-echo sequences have been considered to be the most useful tool for the evaluation of the infiltration of bone marrow in clinical routine along with short tau inversion recovery (STIR),[146,147] yet there is evidence that the detection rate of bone marrow abnormalities and therapy response using MRI can be enhanced by applying techniques such as DWI and DCE-MRI.[144]

DIFFUSION. For the detection of bone marrow infiltration in MM, DW images have been previously generated with EPI sequences (b values: eg, 0, 200, 400, 600, 1000 s/mm^2).[148] As mentioned previously, tissues with high cellularity contain a small interstitial space, which causes restricted water motion.[143,149,150] Therefore, either focal lesions or diffuse tumor cell infiltration of bone marrow can be visualized as hyperintense DW signal. In patients with normal bone marrow, yellow marrow content increases with age, with values between 50% and 60% for subjects older than 61 years, as measured using MRS.[85] Due to the restriction of water diffusion induced by the tightly packed surrounding adipocytes in yellow marrow compared to red marrow, ADC values appear to be low in normal bone marrow with higher yellow marrow content, ranging from 0.2–0.6 $\times$ 10^{-3} mm^2/s, whereas the wide measured range may be explained by experimental differences and differences in fat saturation.[62] In MM progression, water proton diffusivity increases with the increasing water content of the bone marrow due to plasma cell infiltration causing consequent yellow marrow content decrease, therefore ADC values increase, as does the hyperintense signal on DW imaging obtained using high b-values.[149,150] In a previous study assessing mean ADC values before and after therapy in MM patients, ADC increased by 20% in therapy responders.[151] Horger et al found an increase of ADC by 63.9% (range, 8.7–211.3%) 3 weeks after therapy onset in therapy responders,[152] similar to the results of previous studies.[149,150] Therefore, ADC mapping has shown to be a useful tool for the assessment of the disease course of MM.

PERFUSION. Changes in vascular permeability and tumor blood flow through myeloma-induced angiogenesis can be detected using DCE MRI, eg, when using fat-saturated spin-echo T_1-weighted sequences after intravenous administration of contrast medium.[153] DCE MRI techniques can be enhanced through the tracking the temporal passage of the contrast bolus using time—intensity curves (TIC). During the first pass, the contrast agent flows directly from the intravascular to the extracellular space. Afterwards, the contrast agent leaks into tissue and renal clearance occurs; therefore, both the intravascular concentration of contrast agent drops below the interstitial level, and diffusion reverses until all contrast agent is eliminated. TICs therefore allow the semiquantitative[153] and quantitative analysis of DCE imaging using pharmacokinetic models detecting the changes of tissue concentrations of contrast agent over time.[154] Time–intensity curve parameters have been shown to be able to differentiate between different MM groups.[153]

Radiation Therapy Planning and Effects

Insufficiency fractures and hematologic toxicity are clinically important complications of radiation therapy.[155] Bone marrow water/fat quantification has been proposed for measuring the patient-specific bone marrow cellularity distribution in radiation therapy planning.[156] The quantitative evaluation of radiation therapy-associated changes has only been performed in a limited number of studies. Changes of irradiated bone marrow reflecting fatty replacement are traditionally recognized by prolonged T_1 relaxation times.[157]

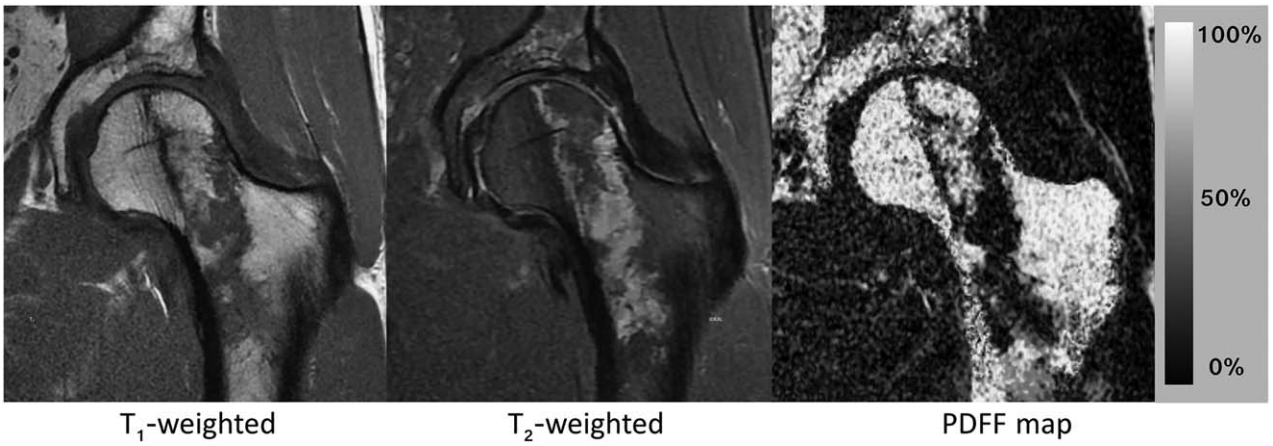

FIGURE 9: MRI of the proximal femur of an HIV-infected male patient. The T_1-weighted TSE (left image) shows low signal in the neck, which can be misinterpreted as hematopoietic red marrow. However, the T_2-weighted fat-suppressed TSE (middle image) shows strong signal from fluid in the same area, suggesting a serous-like lesion. The PDFF map (right image) shows 0% fat in these regions clearly demonstrating the total absence of fat.

Carmona et al recruited 19 subjects who received either highly myelotoxic treatment (radiation and chemotherapy) or less myelotoxic treatment (capecitabine-radiation therapy or no concurrent chemotherapy).[158] Subjects underwent water–fat imaging of the entire spine at baseline, midtreatment, and posttreatment visits. Relative to the reference C3–T9, statistically significant changes in PDFF per visit were observed within L4–S2 (10.1%) and within T10–L3 (3.9%) in the highly myelotoxic group. No significant changes in PDFF were found in the less myelotoxic group. Thus, water–fat imaging is sensitive to changes of bone marrow composition induced by chemoradiation therapy. Similar findings were demonstrated by Bolan et al.[159] They included 13 women with gynecologic malignancies who received radiation and/or chemotherapy. Water–fat imaging was performed at L4 and the femoral neck before treatment and at 6-month follow-up. Fat fraction increases at L4 (16.2%) and the femoral neck (4.5%) were statistically significant. In the future, it remains to be investigated whether these quantitative measurements can improve the risk prediction for hematologic toxicity and insufficiency fractures in patients undergoing radiation therapy.

Future research directions

Quantitative bone marrow MRI allows the noninvasive characterization of bone marrow with a broad range of applications including pathological states of the bone marrow mineralized component, the hematopoietic component, and the fat component. Regarding the fat component, given also the current recent activity on bone marrow adipose tissue physiology,[9] the development of novel noninvasive bone marrow fat biomarkers remains necessary in order to characterize the different types of bone marrow adipocytes.

Regarding the mineralized component, bone marrow characterization remains an important aspect of better understanding the pathophysiology of bone loss induced by both primary and secondary osteoporosis. In addition to the relationship between bone marrow fat fraction and BMD in primary osteoporosis, bone marrow fat changes have been also reported in secondary osteoporosis patients, like patients with chronic kidney disease,[160] in prostate cancer patients treated with androgen deprivation therapy,[161] and in women receiving estrogen.[162]

For example, low BMD and increased fracture risk are increasingly recognized as significant sequelae of HIV

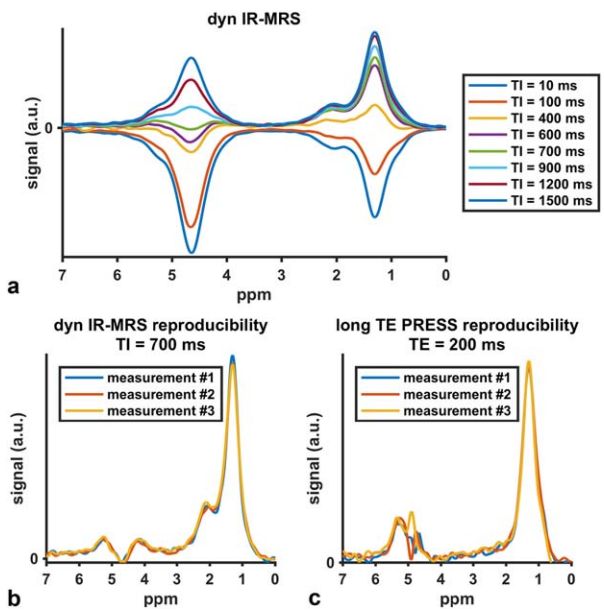

FIGURE 10: IR-MRS data to measure vertebral bone marrow fat unsaturation of a 35-year-old healthy male subject at 3T: (a) dynamic inversion-recovery series with varying inversion time (TI) values from 10 to 1500 msec. Spectra acquired by repeating the same measurement three times for (b) the dynamic IR-MRS (TI = 700 msec, NSA = 8), and (c) the long TE PRESS (TE = 200 msec, NSA = 80). The IR-MRS results in higher SNR spectra than the long-TE PRESS.

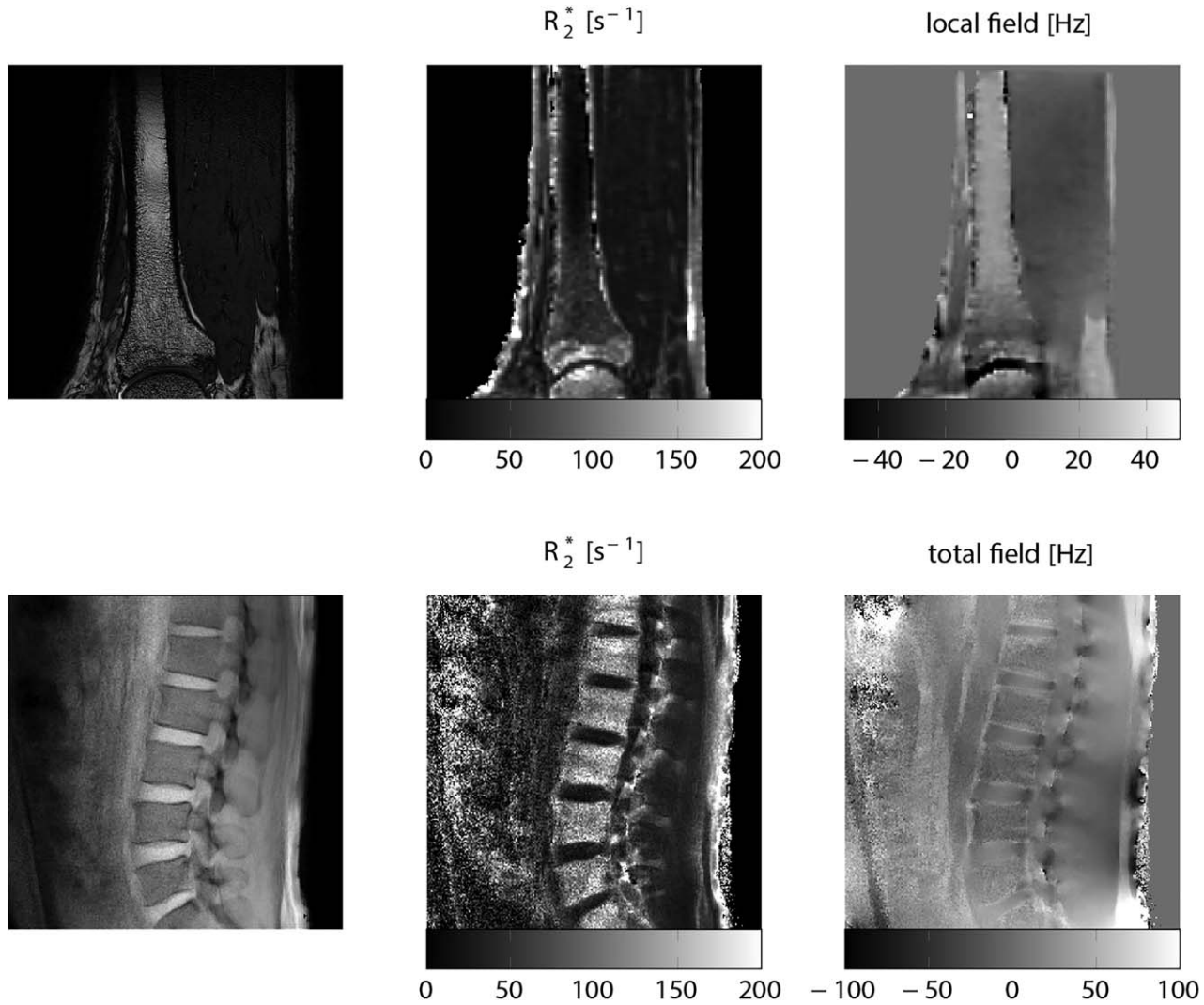

FIGURE 11: Magnetic field contributions induced by trabecular density spatial variation in the distal tibia of a 35-year-old male subject (upper row) and in the lumbar spine of a 36-year-old male subject (lower row). Upper rows are a high-resolution trabecular bone image (left column), an R_2* map (middle column), and a local fieldmap after removal of background fields (right column) of the distal tibia in a healthy subject. Lower row shows single-echo gradient-echo image (left column), an R_2* map (middle column) and total fieldmap (right column) of the lumbar spine in a healthy subject. All data were acquired at 3T, R_2* maps and fieldmaps were generated using chemical shift encoding-based water–fat separation techniques. In the distal tibia, notice the increasing bone density, the increasing R_2*, and the decreasing local field from proximal to distal locations. In the lumbar spine, notice that the higher R_2* and the lower total field between vertebral bodies and neighboring intervertebral discs due to their difference in magnetic susceptibility.

infection and treatment.[163,164] However, while BMD differences between HIV-infected individuals and healthy controls are eliminated by statistical adjustment for weight,[163,165] fracture incidence remains significantly elevated in HIV-infected individuals despite adjustment. Although the etiology of bone quality changes in HIV is unknown, an imbalance in bone and fat cell differentiation may be contributing to low bone quality. However, very little data exist on marrow adiposity in the context of HIV and even a positive relationship between bone quality and marrow adiposity has been previously reported,[166,167] rather than the expected inverse association. One explanation of these findings could be related to abnormalities in the bone marrow in HIV patients that might be incorrectly categorized as hematopoietic or low fat fraction bone marrow. For example, our own preliminary data (Fig. 9) showed that an increased prevalence of marrow serous-like pattern in HIV-infected subjects could be misinterpreted as regions of hematopoietic bone marrow. In Fig. 9, hypointense regions are seen on the T_1-weighted clinical TSE image, However, the fat-suppressed T_2-weighted image reveals the presence of fluid in that region. This finding is confirmed by the PDFF map that shows almost no fat present in this region (hematopoietic marrow in the spine typically contains at least 46% to 66% fat). A high prevalence of serous-like patterns in individuals with HIV has been previously reported.[168] Therefore, these findings emphasize the need for high-resolution fat fraction mapping.

Emerging techniques

Despite the recent progress on reliably and robustly measuring bone marrow fat fraction, many recently used bone marrow imaging biomarkers lack standardization and do not provide a comprehensive characterization of bone marrow properties, which are relevant to bone marrow physiology. The extraction of PDFF instead of SFF and the compensation for unsuppressed fat in bone marrow water ADC measurements constitute simple examples of imaging strategies on how to standardize bone marrow imaging markers. In addition, quantitative bone marrow MRI remains an area where significant new developments have been recently proposed, especially for measuring properties of fatty acid composition and the properties of the trabecular bone matrix.

Despite the significant interest in measuring bone marrow fat unsaturation, the measurement of fat unsaturation in red bone marrow regions remain challenging in the presence of strong water peaks and broad linewidths. Long-TE PRESS and STEAM sequences can reduce the strength of the water peak, but have to significantly prolong the TE in order to minimize J-coupling effects and therefore suffer from reduced SNR. Diffusion-weighted MRS has been proposed as an alternative way to reduce the water peak in regions with low fat fraction,[169] but DW-MRS also requires large b-values to reduce the water peak given the low diffusion coefficient of bone marrow water. An alternative approach to reduce the water peak is using an inversion recovery-prepared MRS (Fig. 10). A joint fitting of variable inversion time spectra could be then employed to extract the water and olefinic fat peaks.

In addition, quantitative magnetic susceptibility (QSM) has been proposed for measuring the magnetic susceptibility in different body parts.[170] Bone marrow QSM might become an alternative in overcoming the limitations of bone marrow T_2^* mapping techniques on indirectly measuring trabecular bone density. Recent applications of QSM techniques have been shown in cortical and trabecular bone regions in the extremities.[171] QSM algorithms rely on the inversion of the susceptibility-induced fieldmap variations. Examples of the fieldmap variations in bone marrow regions with different trabecular bone density are shown in Fig. 11.

In conclusion, quantitative MRI of bone marrow is a valuable tool for the assessment of the physiology and pathophysiology of trabecular bone matrix, the bone marrow adipocytes, and the bone marrow hematopoietic cells. The unique water–fat composition of bone marrow imposes some important technical challenges when measuring the properties of only its water and fat component, and many of the previously used quantitative MRI markers lack standardization, which hinders the comparison of results across studies and their translation to larger-scale clinical studies and eventually the clinical routine.

Acknowledgment

Contract grant sponsor: European Research Council; contract grant number: 677661, ProFatMRI (PI: Karampinos); Contract grant sponsor: Philips Healthcare (PI: Karampinos); Contract grant sponsor: TUM Faculty of Medicine KKF; contract grant number: H01 (PI: Baum); Contract grant sponsor: National Institutes of Health (NIH); contract grant number: NIAMS R01-AR057336 (PI: Krug); Contract grant sponsor: NIH; contract grant numbers: NIAID R01-AI125080 (PIs: Krug, Kazakia) and P30-AI027763 (UCSF Gladstone Institute of Virology & Immunology Center for AIDS Research).

References

1. Nouh MR, Eid AF. Magnetic resonance imaging of the spinal marrow: Basic understanding of the normal marrow pattern and its variant. World J Radiol 2015;7:448–458.
2. Vande Berg BC, Malghem J, Lecouvet FE, Maldague B. Magnetic resonance imaging of normal bone marrow. Eur Radiol 1998;8:1327–1334.
3. Rajmane KC, Schweitzer ME. MR imaging of bone marrow about the knee. Semin Musculoskelet Radiol 2009;13:371–383.
4. Baur-Melnyk A. Magnetic resonance imaging of the bone marrow. Berlin, Heidelberg: Springer; 2013.
5. Moulopoulos LA, Koutoulidis V. Bone marrow MRI: a pattern-based approach. New York: Springer Science & Business Media; 2015.
6. Neumann E. Das Gesetz der Verbreitung des Gelben und rotten Knochenmaarkes. Zentralbl Med Wissensch 1882;20:321–323.
7. Tavassoli M. Marrow adipose cells. Histochemical identification of labile and stable components. Arch Pathol Lab Med 1976;100:16–18.
8. Devlin MJ, Rosen CJ. The bone-fat interface: basic and clinical implications of marrow adiposity. Lancet Diabetes Endocrinol 2015;3:141–147.
9. Scheller EL, Doucette CR, Learman BS, et al. Region-specific variation in the properties of skeletal adipocytes reveals regulated and constitutive marrow adipose tissues. Nat Commun 2015;6:7808.
10. Scheller EL, Rosen CJ. What's the matter with MAT? Marrow adipose tissue, metabolism, and skeletal health. Ann N Y Acad Sci 2014;1311:14–30.
11. Schick F, Bongers H, Jung W-I, et al. Proton relaxation times in human red bone marrow by volume selective magnetic resonance spectroscopy. Appl Magn Reson 1992;3:947–963.
12. Schick F, Bongers H, Jung WI, Skalej M, Lutz O, Claussen CD. Volume-selective proton MRS in vertebral bodies. Magn Reson Med 1992;26:207–217.
13. Baum T, Cordes C, Dieckmeyer M, et al. MR-based assessment of body fat distribution and characteristics. Eur J Radiol 2016;85:1512–1518.
14. Hu HH, Bornert P, Hernando D, et al. ISMRM workshop on fat-water separation: insights, applications and progress in MRI. Magn Reson Med 2012;68:378–388.
15. Hu HH, Kan HE. Quantitative proton MR techniques for measuring fat. NMR Biomed 2013;26:1609–1629.
16. Reeder SB, Cruite I, Hamilton G, Sirlin CB. Quantitative assessment of liver fat with magnetic resonance imaging and spectroscopy. J Magn Reson Imaging 2011;34:729–749.
17. Hernando D, Sharma SD, Aliyari Ghasabeh M, et al. Multisite, multivendor validation of the accuracy and reproducibility of proton-density fat-fraction quantification at 1.5T and 3T using a fat-water phantom. Magn Reson Med 2017;77:1516–1524.
18. Reeder SB, Hu HH, Sirlin CB. Proton density fat-fraction: a standardized MR-based biomarker of tissue fat concentration. J Magn Reson Imaging 2012;36:1011–1014.

19. Hamilton G, Middleton MS, Bydder M, et al. Effect of PRESS and STEAM sequences on magnetic resonance spectroscopic liver fat quantification. J Magn Reson Imaging 2009;30:145–152.
20. Dieckmeyer M, Ruschke S, Cordes C, et al. The need for T(2) correction on MRS-based vertebral bone marrow fat quantification: implications for bone marrow fat fraction age dependence. NMR Biomed 2015;28:432–439.
21. Karampinos DC, Melkus G, Baum T, Bauer JS, Rummeny EJ, Krug R. Bone marrow fat quantification in the presence of trabecular bone: initial comparison between water-fat imaging and single-voxel MRS. Magn Reson Med 2014;71:1158–1165.
22. Hamilton G, Yokoo T, Bydder M, et al. In vivo characterization of the liver fat (1)H MR spectrum. NMR Biomed 2011;24:784–790.
23. Griffith JF, Yeung DK, Antonio GE, et al. Vertebral bone mineral density, marrow perfusion, and fat content in healthy men and men with osteoporosis: dynamic contrast-enhanced MR imaging and MR spectroscopy. Radiology 2005;236:945–951.
24. Griffith JF, Yeung DK, Antonio GE, et al. Vertebral marrow fat content and diffusion and perfusion indexes in women with varying bone density: MR evaluation. Radiology 2006;241:831–838.
25. Griffith JF, Yeung DK, Chow SK, Leung JC, Leung PC. Reproducibility of MR perfusion and (1)H spectroscopy of bone marrow. J Magn Reson Imaging 2009;29:1438–1442.
26. Li X, Kuo D, Schafer AL, et al. Quantification of vertebral bone marrow fat content using 3 Tesla MR spectroscopy: reproducibility, vertebral variation, and applications in osteoporosis. J Magn Reson Imaging 2011;33:974–979.
27. Yeung DK, Griffith JF, Antonio GE, Lee FK, Woo J, Leung PC. Osteoporosis is associated with increased marrow fat content and decreased marrow fat unsaturation: a proton MR spectroscopy study. J Magn Reson Imaging 2005;22:279–285.
28. Pineda AR, Reeder SB, Wen Z, Pelc NJ. Cramer-Rao bounds for three-point decomposition of water and fat. Magn Reson Med 2005; 54:625–635.
29. Yu H, McKenzie CA, Shimakawa A, et al. Multiecho reconstruction for simultaneous water-fat decomposition and T2* estimation. J Magn Reson Imaging 2007;26:1153–1161.
30. Yu H, Shimakawa A, McKenzie CA, Brodsky E, Brittain JH, Reeder SB. Multiecho water-fat separation and simultaneous R2* estimation with multifrequency fat spectrum modeling. Magn Reson Med 2008;60: 1122–1134.
31. Bydder M, Yokoo T, Hamilton G, et al. Relaxation effects in the quantification of fat using gradient echo imaging. Magn Reson Imaging 2008;26:347–359.
32. Hernando D, Liang ZP, Kellman P. Chemical shift-based water/fat separation: a comparison of signal models. Magn Reson Med 2010;64:811–822.
33. Hernando D, Sharma SD, Kramer H, Reeder SB. On the confounding effect of temperature on chemical shift-encoded fat quantification. Magn Reson Med 2014;72:464–470.
34. Wang X, Hernando D, Reeder SB. Sensitivity of chemical shift-encoded fat quantification to calibration of fat MR spectrum. Magn Reson Med 2016;75:845–851.
35. Colgan TJ, Hernando D, Sharma SD, Reeder SB. The effects of concomitant gradients on chemical shift encoded MRI. Magn Reson Med 2016; DOI: 10.1002/mrm.26461 [Epub ahead of print].
36. Ruschke S, Eggers H, Kooijman H, et al. Correction of phase errors in quantitative water-fat imaging using a monopolar time-interleaved multi-echo gradient echo sequence. Magn Reson Med 2016; DOI: 10.1002/mrm.26485 [Epub ahead of print].
37. Yu H, Shimakawa A, Hines CD, et al. Combination of complex-based and magnitude-based multiecho water-fat separation for accurate quantification of fat-fraction. Magn Reson Med 2011;66:199–206.
38. Karampinos DC, Yu H, Shimakawa A, Link TM, Majumdar S. T1-corrected fat quantification using chemical shift-based water/fat separation: application to skeletal muscle. Magn Reson Med 2011;66:1312–1326.
39. Liu CY, McKenzie CA, Yu H, Brittain JH, Reeder SB. Fat quantification with IDEAL gradient echo imaging: correction of bias from T1 and noise. Magn Reson Med 2007;58:354–364.
40. Ren J, Dimitrov I, Sherry AD, Malloy CR. Composition of adipose tissue and marrow fat in humans by 1H NMR at 7 Tesla. J Lipid Res 2008;49:2055–2062.
41. Karampinos DC, Yu H, Shimakawa A, Link TM, Majumdar S. Chemical shift-based water/fat separation in the presence of susceptibility-induced fat resonance shift. Magn Reson Med 2012;68:1495–1505.
42. Yang IY, Cui Y, Wiens CN, Wade TP, Friesen-Waldner LJ, McKenzie CA. Fat fraction bias correction using T1 estimates and flip angle mapping. J Magn Reson Imaging 2014;39:217–223.
43. Karampinos DC, Ruschke S, Dieckmeyer M, et al. Modeling of T2* decay in vertebral bone marrow fat quantification. NMR Biomed 2015;28:1535–1542.
44. Kuhn JP, Hernando D, Meffert PJ, et al. Proton-density fat fraction and simultaneous R2* estimation as an MRI tool for assessment of osteoporosis. Eur Radiol 2013;23:3432–3439.
45. Li G, Xu Z, Gu H, et al. Comparison of chemical shift-encoded water-fat MRI and MR spectroscopy in quantification of marrow fat in postmenopausal females. J Magn Reson Imaging 2017;45:66–73.
46. Le Ster C, Gambarota G, Lasbleiz J, Guillin R, Decaux O, Saint-Jalmes H. Breath-hold MR measurements of fat fraction, T1, and T2* of water and fat in vertebral bone marrow. J Magn Reson Imaging 2016;44:549–555.
47. Le Ster C, Lasbleiz J, Kannengiesser S, Guillin R, Gambarota G, Saint-Jalmes H. A fast method for the quantification of fat fraction and relaxation times: Comparison of five sites of bone marrow. Magn Reson Imaging 2017;39:157–161.
48. Gee CS, Nguyen JT, Marquez CJ, et al. Validation of bone marrow fat quantification in the presence of trabecular bone using MRI. J Magn Reson Imaging 2015;42:539–544.
49. Arentsen L, Yagi M, Takahashi Y, et al. Validation of marrow fat assessment using noninvasive imaging with histologic examination of human bone samples. Bone 2015;72:118–122.
50. Cohen A, Shen W, Dempster DW, et al. Marrow adiposity assessed on transiliac crest biopsy samples correlates with noninvasive measurement of marrow adiposity by proton magnetic resonance spectroscopy ((1)H-MRS) at the spine but not the femur. Osteoporos Int 2015;26:2471–2478.
51. MacEwan IJ, Glembotski NE, D'Lima D, et al. Proton density water fraction as a biomarker of bone marrow cellularity: validation in ex vivo spine specimens. Magn Reson Imaging 2014;32:1097–1101.
52. Bredella MA, Daley SM, Kalra MK, Brown JK, Miller KK, Torriani M. Marrow adipose tissue quantification of the lumbar spine by using dual-energy CT and single-voxel (1)H MR spectroscopy: a feasibility study. Radiology 2015;277:230–235.
53. Singhal V, Miller KK, Torriani M, Bredella MA. Short- and long-term reproducibility of marrow adipose tissue quantification by 1H-MR spectroscopy. Skeletal Radiol 2016;45:221–225.
54. Pansini V, Monnet A, Salleron J, Hardouin P, Cortet B, Cotten A. 3 Tesla (1) H MR spectroscopy of hip bone marrow in a healthy population, assessment of normal fat content values and influence of age and sex. J Magn Reson Imaging 2014;39:369–376.
55. Pansini VM, Monnet A, Salleron J, Penel G, Migaud H, Cotten A. Reproducibility of 1H MR spectroscopy of hip bone marrow at 3 Tesla. J Magn Reson Imaging 2012;36:1445–1449.
56. Lundbom J, Hakkarainen A, Fielding B, et al. Characterizing human adipose tissue lipids by long echo time 1H-MRS in vivo at 1.5 Tesla: validation by gas chromatography. NMR Biomed 2010;23:466–472.
57. Lundbom J, Hakkarainen A, Soderlund S, Westerbacka J, Lundbom N, Taskinen MR. Long-TE 1H MRS suggests that liver fat is more saturated than subcutaneous and visceral fat. NMR Biomed 2011;24:238–245.
58. Troitskaia A, Fallone BG, Yahya A. Long echo time proton magnetic resonance spectroscopy for estimating relative measures of lipid unsaturation at 3 T. J Magn Reson Imaging 2013;37:944–949.

59. Bingolbali A, Fallone BG, Yahya A. Comparison of optimized long echo time STEAM and PRESS proton MR spectroscopy of lipid olefinic protons at 3 Tesla. J Magn Reson Imaging 2015;41:481–486.

60. Machann J, Brechtel IK, Duda SH, Lutz O, Claussen CD, Schick F. Correlation between water content, transverse relaxation, and magnetization transfer in red bone marrow of healthy young subjects In: Proc ISMRM 8th Scientific Meeting & Exhibition, Denver; 2000. p 1945.

61. Biffar A, Dietrich O, Sourbron S, Duerr HR, Reiser MF, Baur-Melnyk A. Diffusion and perfusion imaging of bone marrow. Eur J Radiol 2010; 76:323–328.

62. Dietrich O, Geith T, Reiser MF, Baur-Melnyk A. Diffusion imaging of the vertebral bone marrow. NMR Biomed 2015; DOI: 10.1002/nbm.3333 [Epub ahead of print].

63. Wilm BJ, Svensson J, Henning A, Pruessmann KP, Boesiger P, Kollias SS. Reduced field-of-view MRI using outer volume suppression for spinal cord diffusion imaging. Magn Reson Med 2007;57:625–630.

64. Finsterbusch J. High-resolution diffusion tensor imaging with inner field-of-view EPI. J Magn Reson Imaging 2009;29:987–993.

65. Saritas EU, Cunningham CH, Lee JH, Han ET, Nishimura DG. DWI of the spinal cord with reduced FOV single-shot EPI. Magn Reson Med 2008;60:468–473.

66. Alsop DC. Phase insensitive preparation of single-shot RARE: application to diffusion imaging in humans. Magn Reson Med 1997;38:527–533.

67. Wu EX, Buxton RB. Effect of diffusion on the steady-state magnetization with pulsed field gradients. J Magn Reson 1990;90:243–253.

68. Hernando D, Karampinos DC, King KF, et al. Removal of olefinic fat chemical shift artifact in diffusion MRI. Magn Reson Med 2011;65: 692–701.

69. Williams SE, Heemskerk AM, Welch EB, Li K, Damon BM, Park JH. Quantitative effects of inclusion of fat on muscle diffusion tensor MRI measurements. J Magn Reson Imaging 2013;38:1292–1297.

70. Hansmann J, Hernando D, Reeder SB. Fat confounds the observed apparent diffusion coefficient in patients with hepatic steatosis. Magn Reson Med 2013;69:545–552.

71. Dieckmeyer M, Ruschke S, Eggers H, et al. ADC quantification of the vertebral bone marrow water component: removing the confounding effect of residual fat. Magn Reson Med 2016; DOI: 10.1002/mrm.26550 [Epub ahead of print].

72. Burakiewicz J, Hooijmans MT, Webb AG, Verschuuren JJ, Niks EH, Kan HE. Improved olefinic fat suppression in skeletal muscle DTI using a magnitude-based dixon method. Magn Reson Med 2017; DOI: 10.1002/mrm.26655 [Epub ahead of print].

73. Biffar A, Schmidt GP, Sourbron S, et al. Quantitative analysis of vertebral bone marrow perfusion using dynamic contrast-enhanced MRI: initial results in osteoporotic patients with acute vertebral fracture. J Magn Reson Imaging 2011;33:676–683.

74. Schick F, Forster J, Einsele H, Weiss B, Lutz O, Claussen CD. Magnetization transfer in hemopoietic bone marrow examined by localized proton spectroscopy. Magn Reson Med 1995;34:792–802.

75. Wehrli FW. Structural and functional assessment of trabecular and cortical bone by micro magnetic resonance imaging. J Magn Reson Imaging 2007;25:390–409.

76. Wehrli FW, Song HK, Saha PK, Wright AC. Quantitative MRI for the assessment of bone structure and function. NMR Biomed 2006;19: 731–764.

77. Majumdar S, Genant HK. In vivo relationship between marrow T2* and trabecular bone density determined with a chemical shift-selective asymmetric spin-echo sequence. J Magn Reson Imaging 1992;2:209–219.

78. Chung H, Wehrli FW, Williams JL, Kugelmass SD. Relationship between NMR transverse relaxation, trabecular bone architecture, and strength. Proc Natl Acad Sci U S A 1993;90:10250–10254.

79. Ma J, Wehrli FW. Method for image-based measurement of the reversible and irreversible contribution to the transverse-relaxation rate. J Magn Reson B 1996;111:61–69.

80. Wehrli FW, Ma J, Hopkins JA, Song HK. Measurement of R'2 in the presence of multiple spectral components using reference spectrum deconvolution. J Magn Reson 1998;131:61–68.

81. Wehrli FW, Hopkins JA, Hwang SN, Song HK, Snyder PJ, Haddad JG. Cross-sectional study of osteopenia with quantitative MR imaging and bone densitometry. Radiology 2000;217:527–538.

82. Aoki T, Yamaguchi S, Kinoshita S, Hayashida Y, Korogi Y. Quantification of bone marrow fat content using iterative decomposition of water and fat with echo asymmetry and least-squares estimation (IDEAL): reproducibility, site variation and correlation with age and menopause. Br J Radiol 2016;89:20150538.

83. Baum T, Yap SP, Dieckmeyer M, et al. Assessment of whole spine vertebral bone marrow fat using chemical shift-encoding based water-fat MRI. J Magn Reson Imaging 2015;42:1018–1023.

84. Griffith JF, Yeung DK, Ma HT, Leung JC, Kwok TC, Leung PC. Bone marrow fat content in the elderly: a reversal of sex difference seen in younger subjects. J Magn Reson Imaging 2012;36:225–230.

85. Kugel H, Jung C, Schulte O, Heindel W. Age- and sex-specific differences in the 1H-spectrum of vertebral bone marrow. J Magn Reson Imaging 2001;13:263–268.

86. Liney GP, Bernard CP, Manton DJ, Turnbull LW, Langton CM. Age, gender, and skeletal variation in bone marrow composition: a preliminary study at 3.0 Tesla. J Magn Reson Imaging 2007;26:787–793.

87. Roldan-Valadez E, Pina-Jimenez C, Favila R, Rios C. Gender and age groups interactions in the quantification of bone marrow fat content in lumbar spine using 3T MR spectroscopy: a multivariate analysis of covariance (Mancova). Eur J Radiol 2013;82:e697–e702.

88. Schellinger D, Lin CS, Fertikh D, et al. Normal lumbar vertebrae: anatomic, age, and sex variance in subjects at proton MR spectroscopy—initial experience. Radiology 2000;215:910–916.

89. Chen WT, Shih TT, Chen RC, et al. Vertebral bone marrow perfusion evaluated with dynamic contrast-enhanced MR imaging: significance of aging and sex. Radiology 2001;220:213–218.

90. Hillengass J, Stieltjes B, Bauerle T, et al. Dynamic contrast-enhanced magnetic resonance imaging (DCE-MRI) and diffusion-weighted imaging of bone marrow in healthy individuals. Acta Radiol 2011;52:324–330.

91. Yeung DK, Wong SY, Griffith JF, Lau EM. Bone marrow diffusion in osteoporosis: evaluation with quantitative MR diffusion imaging. J Magn Reson Imaging 2004;19:222–228.

92. Group WS. Assessment of fracture risk and its application to screening for postmenopausal osteoporosis. Report of a WHO Study Group. World Health Organ Tech Rep Ser 1994;843:1–129.

93. Burge R, Dawson-Hughes B, Solomon DH, Wong JB, King A, Tosteson A. Incidence and economic burden of osteoporosis-related fractures in the United States, 2005–2025. J Bone Miner Res 2007;22: 465–475.

94. Hernlund E, Svedbom A, Ivergard M, et al. Osteoporosis in the European Union: medical management, epidemiology and economic burden. A report prepared in collaboration with the International Osteoporosis Foundation (IOF) and the European Federation of Pharmaceutical Industry Associations (EFPIA). Arch Osteoporos 2013;8: 136.

95. Schuit SC, van der Klift M, Weel AE, et al. Fracture incidence and association with bone mineral density in elderly men and women: the Rotterdam Study. Bone 2004;34:195–202.

96. Siris ES, Chen YT, Abbott TA, et al. Bone mineral density thresholds for pharmacological intervention to prevent fractures. Arch Intern Med 2004;164:1108–1112.

97. Kanis JA, Oden A, Johansson H, Borgstrom F, Strom O, McCloskey E. FRAX and its applications to clinical practice. Bone 2009;44:734–743.

98. Baum T, Karampinos DC, Liebl H, Rummeny EJ, Waldt S, Bauer JS. High-resolution bone imaging for osteoporosis diagnostics and therapy monitoring using clinical MDCT and MRI. Curr Med Chem 2013; 20:4844–4852.

99. Link TM. Osteoporosis imaging: state of the art and advanced imaging. Radiology 2012;263:3–17.

100. Cordes C, Baum T, Dieckmeyer M, et al. MR-based assessment of bone marrow fat in osteoporosis, diabetes, and obesity. Front Endocrinol (Lausanne) 2016;7:74.

101. Paccou J, Hardouin P, Cotten A, Penel G, Cortet B. The role of bone marrow fat in skeletal health: usefulness and perspectives for clinicians. J Clin Endocrinol Metab 2015;100:3613–3621.

102. Rosen CJ, Bouxsein ML. Mechanisms of disease: is osteoporosis the obesity of bone? Nat Clin Pract Rheumatol 2006;2:35–43.

103. Karampinos DC, Ruschke S, Gordijenko O, et al. Association of MRS-based vertebral bone marrow fat fraction with bone strength in a human in vitro model. J Osteoporos 2015;2015:152349.

104. Ergen FB, Gulal G, Yildiz AE, Celik A, Karakaya J, Aydingoz U. Fat fraction estimation of the vertebrae in females using the T2*-IDEAL technique in detection of reduced bone mineralization level: comparison with bone mineral densitometry. J Comput Assist Tomogr 2014;38:320–324.

105. Li GW, Xu Z, Chen QW, et al. Quantitative evaluation of vertebral marrow adipose tissue in postmenopausal female using MRI chemical shift-based water-fat separation. Clin Radiol 2014;69: 254–262.

106. Martin J, Nicholson G, Cowin G, Ilente C, Wong W, Kennedy D. Rapid determination of vertebral fat fraction over a large range of vertebral bodies. J Med Imaging Radiat Oncol 2014;58:155–163.

107. Schwartz AV, Sigurdsson S, Hue TF, et al. Vertebral bone marrow fat associated with lower trabecular BMD and prevalent vertebral fracture in older adults. J Clin Endocrinol Metab 2013;98:2294–2300.

108. Patsch JM, Li X, Baum T, et al. Bone marrow fat composition as a novel imaging biomarker in postmenopausal women with prevalent fragility fractures. J Bone Miner Res 2013;28:1721–1728.

109. Hatipoglu HG, Selvi A, Ciliz D, Yuksel E. Quantitative and diffusion MR imaging as a new method to assess osteoporosis. AJNR Am J Neuroradiol 2007;28:1934–1937.

110. Liu Y, Tang GY, Tang RB, Peng YF, Li W. Assessment of bone marrow changes in postmenopausal women with varying bone densities: magnetic resonance spectroscopy and diffusion magnetic resonance imaging. Chin Med J (Engl) 2010;123:1524–1527.

111. Tang GY, Lv ZW, Tang RB, et al. Evaluation of MR spectroscopy and diffusion-weighted MRI in detecting bone marrow changes in postmenopausal women with osteoporosis. Clin Radiol 2010;65:377–381.

112. Burkhardt R, Kettner G, Bohm W, et al. Changes in trabecular bone, hematopoiesis and bone marrow vessels in aplastic anemia, primary osteoporosis, and old age: a comparative histomorphometric study. Bone 1987;8:157–164.

113. Shih TT, Liu HC, Chang CJ, Wei SY, Shen LC, Yang PC. Correlation of MR lumbar spine bone marrow perfusion with bone mineral density in female subjects. Radiology 2004;233:121–128.

114. Griffith JF, Yeung DK, Tsang PH, et al. Compromised bone marrow perfusion in osteoporosis. J Bone Miner Res 2008;23:1068–1075.

115. Wang YX, Griffith JF, Kwok AW, et al. Reduced bone perfusion in proximal femur of subjects with decreased bone mineral density preferentially affects the femoral neck. Bone 2009;45:711–715.

116. Bredella MA, Torriani M, Ghomi RH, et al. Vertebral bone marrow fat is positively associated with visceral fat and inversely associated with IGF-1 in obese women. Obesity (Silver Spring) 2011;19: 49–53.

117. Bredella MA, Gill CM, Gerweck AV, et al. Ectopic and serum lipid levels are positively associated with bone marrow fat in obesity. Radiology 2013;269:534–541.

118. Cordes C, Dieckmeyer M, Ott B, et al. MR-detected changes in liver fat, abdominal fat, and vertebral bone marrow fat after a four-week calorie restriction in obese women. J Magn Reson Imaging 2015;42: 1272–1280.

119. Schafer AL, Li X, Schwartz AV, et al. Changes in vertebral bone marrow fat and bone mass after gastric bypass surgery: A pilot study. Bone 2015;74:140–145.

120. Sheu Y, Amati F, Schwartz AV, et al. Vertebral bone marrow fat, bone mineral density and diabetes: The Osteoporotic Fractures in Men (MrOS) study. Bone 2017;97:299–305.

121. Baum T, Yap SP, Karampinos DC, et al. Does vertebral bone marrow fat content correlate with abdominal adipose tissue, lumbar spine bone mineral density, and blood biomarkers in women with type 2 diabetes mellitus? J Magn Reson Imaging 2012;35:117–124.

122. Bredella MA, Fazeli PK, Miller KK, et al. Increased bone marrow fat in anorexia nervosa. J Clin Endocrinol Metab 2009;94:2129–2136.

123. Slade JM, Coe LM, Meyer RA, McCabe LR. Human bone marrow adiposity is linked with serum lipid levels not T1-diabetes. J Diabetes Complications 2012;26:1–9.

124. Grey A, Beckley V, Doyle A, et al. Pioglitazone increases bone marrow fat in type 2 diabetes: results from a randomized controlled trial. Eur J Endocrinol 2012;166:1087–1091.

125. Hansen EJ, Simony A, Carreon L, Andersen MO. Rate of unsuspected malignancy in patients with vertebral compression fracture undergoing percutaneous vertebroplasty. Spine (Phila Pa 1976) 2016;41:549–552.

126. Jung HS, Jee WH, McCauley TR, Ha KY, Choi KH. Discrimination of metastatic from acute osteoporotic compression spinal fractures with MR imaging. Radiographics 2003;23:179–187.

127. Shih TT, Huang KM, Li YW. Solitary vertebral collapse: distinction between benign and malignant causes using MR patterns. J Magn Reson Imaging 1999;9:635–642.

128. Geith T, Schmidt G, Biffar A, et al. Comparison of qualitative and quantitative evaluation of diffusion-weighted MRI and chemical-shift imaging in the differentiation of benign and malignant vertebral body fractures. AJR Am J Roentgenol 2012;199:1083–1092.

129. Erly WK, Oh ES, Outwater EK. The utility of in-phase/opposed-phase imaging in differentiating malignancy from acute benign compression fractures of the spine. AJNR Am J Neuroradiol 2006;27:1183–1188.

130. Ragab Y, Emad Y, Gheita T, et al. Differentiation of osteoporotic and neoplastic vertebral fractures by chemical shift {in-phase and out-of phase} MR imaging. Eur J Radiol 2009;72:125–133.

131. Yoo HJ, Hong SH, Kim DH, et al. Measurement of fat content in vertebral marrow using a modified dixon sequence to differentiate benign from malignant processes. J Magn Reson Imaging 2016;DOI: 10.1002/jmri.25496 [Epub ahead of print].

132. Raya JG, Dietrich O, Reiser MF, Baur-Melnyk A. Methods and applications of diffusion imaging of vertebral bone marrow. J Magn Reson Imaging 2006;24:1207–1220.

133. Castillo M, Arbelaez A, Smith JK, Fisher LL. Diffusion-weighted MR imaging offers no advantage over routine noncontrast MR imaging in the detection of vertebral metastases. AJNR Am J Neuroradiol 2000;21:948–953.

134. Geith T, Schmidt G, Biffar A, et al. Quantitative evaluation of benign and malignant vertebral fractures with diffusion-weighted MRI: what is the optimum combination of b values for ADC-based lesion differentiation with the single-shot turbo spin-echo sequence? AJR Am J Roentgenol 2014;203:582–588.

135. Tokuda O, Hayashi N, Taguchi K, Matsunaga N. Dynamic contrast-enhanced perfusion MR imaging of diseased vertebrae: analysis of three parameters and the distribution of the time-intensity curve patterns. Skeletal Radiol 2005;34:632–638.

136. Biffar A, Sourbron S, Schmidt G, et al. Measurement of perfusion and permeability from dynamic contrast-enhanced MRI in normal and pathological vertebral bone marrow. Magn Reson Med 2010;64: 115–124.

137. Geith T, Biffar A, Schmidt G, et al. Quantitative analysis of acute benign and malignant vertebral body fractures using dynamic contrast-enhanced MRI. AJR Am J Roentgenol 2013;200:W635–643.

138. Machann J, Stefan N, Schick F. (1)H MR spectroscopy of skeletal muscle, liver and bone marrow. Eur J Radiol 2008;67:275–284.

139. Schick F, Einsele H, Lutz O, Claussen CD. Lipid selective MR imaging and localized 1H spectroscopy of bone marrow during therapy of leukemia. Anticancer Res 1996;16:1545–1551.

140. Kyle RA, Durie BG, Rajkumar SV, et al. Monoclonal gammopathy of undetermined significance (MGUS) and smoldering (asymptomatic) multiple myeloma: IMWG consensus perspectives risk factors for progression and guidelines for monitoring and management. Leukemia 2010;24:1121–1127.

141. Smith D, Yong K. Multiple myeloma. BMJ 2013;346:f3863.

142. Rajkumar SV, Dimopoulos MA, Palumbo A, et al. International Myeloma Working Group updated criteria for the diagnosis of multiple myeloma. Lancet Oncol 2014;15:e538–548.

143. Padhani AR, Khan AA. Diffusion-weighted (DW) and dynamic contrast-enhanced (DCE) magnetic resonance imaging (MRI) for monitoring anticancer therapy. Target Oncol 2010;5:39–52.

144. Caers J, Withofs N, Hillengass J, et al. The role of positron emission tomography-computed tomography and magnetic resonance imaging in diagnosis and follow up of multiple myeloma. Haematologica 2014;99:629–637.

145. Hillengass J, Landgren O. Challenges and opportunities of novel imaging techniques in monoclonal plasma cell disorders: imaging "early myeloma." Leuk Lymphoma 2013;54:1355–1363.

146. Shah LM, Hanrahan CJ. MRI of spinal bone marrow: part I, techniques and normal age-related appearances. AJR Am J Roentgenol 2011;197:1298–1308.

147. Silva JR Jr, Hayashi D, Yonenaga T, et al. MRI of bone marrow abnormalities in hematological malignancies. Diagn Interv Radiol 2013;19:393–399.

148. Khoo MM, Tyler PA, Saifuddin A, Padhani AR. Diffusion-weighted imaging (DWI) in musculoskeletal MRI: a critical review. Skeletal Radiol 2011;40:665–681.

149. Dutoit JC, Vanderkerken MA, Anthonissen J, Dochy F, Verstraete KL. The diagnostic value of SE MRI and DWI of the spine in patients with monoclonal gammopathy of undetermined significance, smouldering myeloma and multiple myeloma. Eur Radiol 2014;24:2754–2765.

150. Padhani AR, van Ree K, Collins DJ, D'Sa S, Makris A. Assessing the relation between bone marrow signal intensity and apparent diffusion coefficient in diffusion-weighted MRI. AJR Am J Roentgenol 2013;200:163–170.

151. Giles SL, Messiou C, Collins DJ, et al. Whole-body diffusion-weighted MR imaging for assessment of treatment response in myeloma. Radiology 2014;271:785–794.

152. Horger M, Weisel K, Horger W, Mroue A, Fenchel M, Lichy M. Whole-body diffusion-weighted MRI with apparent diffusion coefficient mapping for early response monitoring in multiple myeloma: preliminary results. AJR Am J Roentgenol 2011;196:W790–795.

153. Dutoit JC, Vanderkerken MA, Verstraete KL. Value of whole body MRI and dynamic contrast enhanced MRI in the diagnosis, follow-up and evaluation of disease activity and extent in multiple myeloma. Eur J Radiol 2013;82:1444–1452.

154. Garcia-Figueiras R, Padhani AR, Beer AJ, et al. Imaging of tumor angiogenesis for radiologists. Part 1: Biological and technical basis. Curr Probl Diagn Radiol 2015;44:407–424.

155. Higham CE, Faithfull S. Bone health and pelvic radiotherapy. Clin Oncol (R Coll Radiol) 2015;27:668–678.

156. Pichardo JC, Milner RJ, Bolch WE. MRI measurement of bone marrow cellularity for radiation dosimetry. J Nucl Med 2011;52:1482–1489.

157. Sugimura H, Kisanuki A, Tamura S, Kihara Y, Watanabe K, Sumiyoshi A. Magnetic resonance imaging of bone marrow changes after irradiation. Invest Radiol 1994;29:35–41.

158. Carmona R, Pritz J, Bydder M, et al. Fat composition changes in bone marrow during chemotherapy and radiation therapy. Int J Radiat Oncol Biol Phys 2014;90:155–163.

159. Bolan PJ, Arentsen L, Sueblinvong T, et al. Water-fat MRI for assessing changes in bone marrow composition due to radiation and chemotherapy in gynecologic cancer patients. J Magn Reson Imaging 2013;38:1578–1584.

160. Moorthi RN, Fadel W, Eckert GJ, Ponsler-Sipes K, Moe SM, Lin C. Bone marrow fat is increased in chronic kidney disease by magnetic resonance spectroscopy. Osteoporos Int 2015;26:1801–1807.

161. Martin J, Arm J, Smart J, et al. Spinal multiparametric MRI and DEXA changes over time in men with prostate cancer treated with androgen deprivation therapy: a potential imaging biomarker of treatment toxicity. Eur Radiol 2017;27:995–1003.

162. Limonard EJ, Veldhuis-Vlug AG, van Dussen L, et al. Short-term effect of estrogen on human bone marrow fat. J Bone Miner Res 2015;30:2058–2066.

163. Arnsten JH, Freeman R, Howard AA, Floris-Moore M, Lo Y, Klein RS. Decreased bone mineral density and increased fracture risk in aging men with or at risk for HIV infection. AIDS 2007;21:617–623.

164. Triant VA, Brown TT, Lee H, Grinspoon SK. Fracture prevalence among human immunodeficiency virus (HIV)-infected versus non-HIV-infected patients in a large U.S. healthcare system. J Clin Endocrinol Metab 2008;93:3499–3504.

165. Prior J, Burdge D, Maan E, et al. Fragility fractures and bone mineral density in HIV positive women: a case-control population-based study. Osteoporos Int 2007;18:1345–1353.

166. Huang JS, Mulkern RV, Grinspoon S. Reduced intravertebral bone marrow fat in HIV-infected men. AIDS 2002;16:1265–1269.

167. Mulkern RV, Huang J, Vajapeyam S, Packard AB, Oshio K, Grinspoon S. Fat fractions and spectral T2 values in vertebral bone marrow in HIV- and non-HIV-infected men: a 1H spectroscopic imaging study. Magn Reson Med 2004;52:552–558.

168. Garcia AI, Milinkovic A, Tomas X, et al. MRI signal changes of the bone marrow in HIV-infected patients with lipodystrophy: correlation with clinical parameters. Skeletal Radiol 2011;40:1295–1301.

169. Ruschke S, Kienberger H, Baum T, et al. Diffusion-weighted stimulated echo acquisition mode (DW-STEAM) MR spectroscopy to measure fat unsaturation in regions with low proton-density fat fraction. Magn Reson Med 2016;75:32–41.

170. Wang Y, Spincemaille P, Liu Z, et al. Clinical quantitative susceptibility mapping (QSM) : Biometal imaging and its emerging roles in patient care. J Magn Reson Imaging 2017; DOI: 10.1002/jmri.25693 [Epub ahead of print].

171. Dimov AV, Liu Z, Spincemaille P, Prince MR, Du J, Wang Y. Bone quantitative susceptibility mapping using a chemical species-specific R2* signal model with ultrashort and conventional echo data. Magn Reson Med 2017; DOI: 10.1002/mrm.26648 [Epub ahead of print].